ETH
Eidgenössische Technische Hochschule Zürich
Swiss Federal Institute of Technology Zurich

Trapped Ion Quantum
Information Group

Master's Thesis

Theoretical aspects of H_2^+ spectroscopy

Luis Carlos González Hofmann

Master of Science in Physics
Trapped Ion Quantum Information Group
Swiss Federal Institute of Technology (ETH) Zurich

Supervision:
Dr. Fabian Schmid
Dr. Daniel Kienzler
Prof. Dr. Jonathan Home

Zürich, July 2024

Abstract

The hydrogen molecular ion (H_2^+) is the simplest molecule and an essential system for testing fundamental constants and validating quantum theories due to the high precision achievable in its theoretical calculations. Despite its apparent simplicity, the precise control and understanding of H_2^+ present significant challenges.

This thesis provides a detailed theoretical analysis of the hyperfine structure of H_2^+, calculating transition matrix elements for magnetic dipole, two-photon, and quadrupole transitions. It also evaluates energy level shifts including quadrupole, DC Stark, and light-induced shifts. These analyses apply to the ro-vibrational levels of both para-H_2^+ and ortho-H_2^+.

The theoretical framework developed here is applicable to all bond states. Explicit numerical results for the transition matrix elements and energy level shifts are provided for different ro-vibrational levels, improving the accuracy of theoretical predictions for high-precision spectroscopy for H_2^+.

Acknowledgements

First and foremost, I would like to express my deepest gratitude to Fabian Schmid. Your continuous support, insightful comments, and invaluable guidance have been instrumental in shaping this thesis. Your willingness to always answer my questions, provide feedback, and work through challenges with me has made an enormous difference in my research journey. I could not have completed this work without your expertise and dedication.

I would also like to thank my official supervisors, Prof. Jonathan Home and Daniel Kienzler. Prof. Home, thank you for giving me the opportunity to pursue my thesis within your group. Dr. Kienzler, your support and feedback during our subgroup meetings were invaluable.

My heartfelt thanks go to the entire molecules subgroup. The weekly meetings we had were incredibly helpful, providing me with the constructive feedback and support I needed to progress in my work.

Furthermore, I would like to extend my gratitude to the entire TIQI group. The great environment within the group made my research experience enjoyable and enriching.

Lastly, I am grateful to my family and friends for their unwavering support and encouragement throughout this journey. Your belief in me has been a source of strength and motivation.

Thank you all for your contributions, support, and encouragement. This thesis would not have been possible without you.

Contents

Chapter 1

Introduction

The hydrogen molecular ion H_2^+ consists of two protons and one electron, forming a simple yet profoundly important system in molecular physics and quantum chemistry. The study of H_2^+ is compelling due to its fundamental nature and the precision with which its properties can be calculated and measured. As the most basic molecular ion, H_2^+ serves as a critical test-bed for theories of molecular structure and dynamics, quantum electrodynamics (QED), and the interactions between particles at the quantum level. Insights gained from H_2^+ spectroscopy not only advance our understanding of fundamental physical principles but also enhance the accuracy of spectroscopic techniques used to probe more complex systems.

To achieve a deeper understanding of H_2^+, we aim to study its theoretical aspects with a focus on determining theoretical transition frequencies accurately. This involves investigating the fine structure and hyperfine transitions of the ion, providing a framework for comparison with experimental data to validate our theoretical models. Any discrepancies between theory and experiment may reveal the need for refined models or uncover interactions not accounted for in existing theories, such as subtle nuclear spin interactions beyond the standard model.

Experimentally the H_2^+ molecule poses many challenges. Many of the methods employed on other systems (such as direct laser cooling, internal readout by state-dependent fluorescence detection, and state preparation by optical pumping) cannot be employed. In [1] the first steps required for quantum logic spectroscopy are demonstrated, following a method proposed in earlier publications, which involves co-trapping and sideband cooling a H_2^+ - $^9Be^+$ ion pair in a cryogenic Paul trap. This trap is shown in figure 1.1.

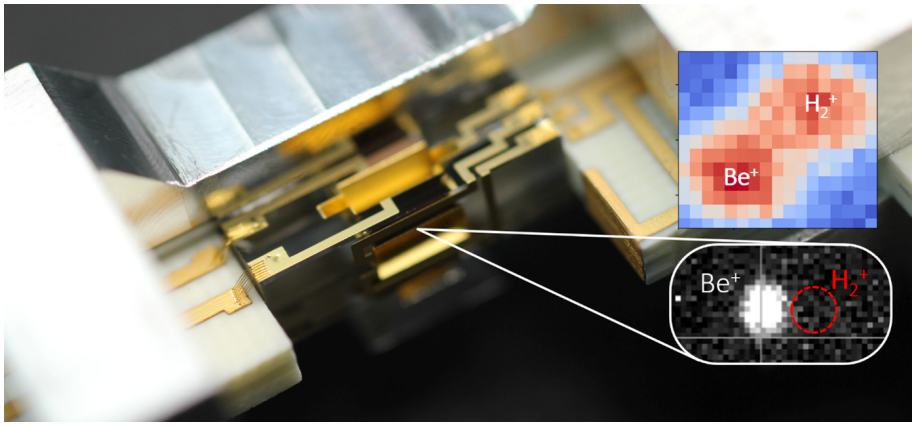

Figure 1.1: The ion trap at TIQI. The lower inset shows a fluorescence image of a single trapped Be^+ ion. The co-trapped H_2^+ ion is invisible, but its presence can be inferred from the position and mechanical resonances of the Be^+ ion. The upper inset shows a quantum logic signal, making the H_2^+ visible. This image is taken from the TIQI homepage.

In chapter 2 we discuss the hyperfine structure of the H_2^+ ion. We present a detailed discussion on the effective spin Hamiltonian, followed by the computation of its matrix elements. The primary goal is to determine the hyperfine basis states, which are foundational for understanding the ion's energy levels and interactions. This exploration provides a theoretical framework essential for high-precision spectroscopic analysis and for interpreting experimental data in the context of the H_2^+ ion.

In chapter 3 we examine the hyperfine structure of beryllium. Understanding the hyperfine interactions and energy levels of $^9Be^+$ is critical for characterizing the magnetic field environment within the trap, which is required for high-precision spectroscopic measurements of H_2^+. By analyzing the hyperfine structure of $^9Be^+$, we can effectively monitor and control the magnetic field.

In chapter 4 we explore the intricate nature of hyperfine transitions in H_2^+, which are essential for comprehending the ion's spectroscopic behavior. We begin with magnetic field insensitive transitions, highlighting their role in achieving high-precision measurements. The chapter further examines various transitions, including magnetic dipole (M1), two-photon (2E1), and electric quadrupole (E2) transitions, discussing their theoretical foundations.

In chapter 5, we address various systematic frequency shifts that affect the accuracy of spectroscopic measurements of H_2^+. We investigate the quadrupole shift, the DC Stark shift, and light-induced shifts, discussing their origins and theoretical characterization. Understanding and mitigating these shifts is crucial not only

for precise hyperfine transitions but also for accurate ro-vibrational transitions, thereby enhancing the overall reliability of H_2^+ spectroscopic techniques.

Finally, in the appendix, we provide supplementary theoretical and computational details that support the main content of the thesis. This includes an in-depth discussion on the angular momentum structure, the coupling of angular momenta, irreducible tensor operators, and reduced matrix elements in Appendix A. We also cover the labeling of eigenstates for the lowest levels in Appendix B and the calculation of transition probabilities for magnetic dipole (M1), two-photon (2E1), and electric quadrupole (E2) transitions in Appendix C. These additional details provide a rigorous foundation for the analyses presented in the earlier chapters, underpinning the study of hyperfine transitions in H_2^+.

1.1 Non-relativistic Hamiltonian

In order to better understand the labeling of states and to gain a basis of knowledge for this molecule we will briefly talk about the non-relativistic Hamiltonian and the states we obtain, when we look for its eigenfunctions. As mentioned before, the H_2^+ molecule consists of two protons and one electron that interact via the Coulomb interaction. With this notation, we can express the non-relativistic Hamiltonian H_0 of the system as:

$$H_0 = \frac{\vec{p_1}^2 + \vec{p_2}^2}{2m_p} + \frac{\vec{p_e}^2}{2m_e} + \frac{e^2}{4\pi\epsilon_0}(-\frac{1}{r_1} - \frac{1}{r_2} + \frac{1}{r_{12}}), \tag{1.1}$$

Where m_p and m_e are the masses of a proton and electron respectively. Here r_i $(i = 1, 2)$ are the distances between the electron and each proton, and r_{12} is the distance between the two protons. This Hamiltonian is not analytically solvable. Using the Born-Oppenheimer approximation this problem has been solved as early as 1930, and the energy levels have been calculated in [8]. In the recent years, the nonrelativistic problem has been solved numerically to essentially arbitrary precision (for example in [2] or [3]) following the methodology developed in [4]. However, the uncertainties in the relativistic corrections now dominate, limiting the overall precision.

The molecular states of the H_2^+ ion, particularly the formalism involving the Σ_g, Σ_u, and Π bands, can be understood through the context of molecular orbital theory and the Born-Oppenheimer approximation. In molecular systems, such as H_2^+, the orbitals are classified based on their symmetry properties and quantum numbers. In analogy to the orbitals of an atom, that are classified according to m, the quantum number for the z-component of the angular momentum ($m = 0, 1, ...$

correspond to σ, π,...); for a molecule the classification is in capital letters (Σ, Π,...). For this system, only the Σ orbitals are of relevance, as for all the other bands, all states lie above the dissociation energy, so they do not posses any bond states. These Σ orbitals have cylindrical symmetry around the molecular axis.

The Σ band is split into two, the subscripts on Σ_g (gerade) and Σ_u (ungerade) refer to the behavior of these orbitals under inversion through the center of the molecule. g indicates that the orbital is symmetric, while u indicates that the orbital is anti-symmetric under this inversion. For the H_2^+ ion, it is established that most of the bound states are in the Σ_g band, except for a four loosely bound Σ_u states.

Within each band, the energy levels are split according to quantized types of motion, specifically vibrations and rotations. Firstly, the vibrational levels, denoted by ν, exhibit larger splittings and can take on values ranging from 0 up to a maximum of 19 for the bond states. Within each vibrational level, the states are further split into rotational levels, L, which can take values up to 41 for the bond states. Therefore, in each band, the states can be labeled according to the so-called ro-vibrational level (ν, L), which fully characterizes the non-relativistic electronic ground state of H_2^+. The full list of all the states with their energies can be found in the tables in [8].

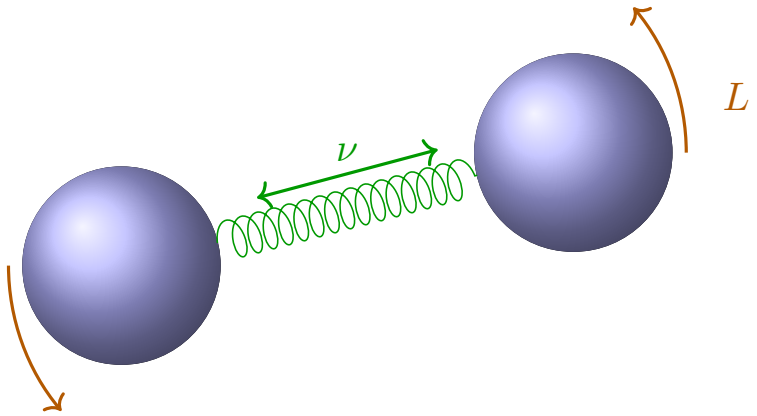

Figure 1.2: Schematic representation of a H_2^+ molecule, illustrating vibrational motion (ν) and rotational motion (L) of the molecule.

Chapter 2

The hyperfine structure of H_2^+

The hyperfine structure of the H_2^+ molecular ion arises due to the interactions between the magnetic moments caused by the different angular momenta of the particles within the molecule. This section treats the theoretical framework used to understand and calculate these hyperfine energy levels. By incorporating both relativistic corrections and external magnetic fields, the resulting Hamiltonian provides a comprehensive view of the energy splitting.

For each ro-vibrational level (ν, L), the effect of these interactions is encoded into an effective spin Hamiltonian H_{eff}. The level is split into hyperfine states, which correspond to the eigenvectors of this Hamiltonian matrix. The hyperfine energy correction for each state is the eigenvalue corresponding to this eigenvector.

The sections below explore the key components contributing to the hyperfine Hamiltonian. The angular momentum coupling scheme is first introduced, detailing how the spins and orbital angular momenta of the proton and electron are combined to form total angular momentum states. This sets the foundation for understanding the subsequent terms in the Hamiltonian.

Following this, we discuss the effective spin Hamiltonian, which includes the spin-spin interactions between the electron and proton, the electron spin-rotation interaction, and the orbit-nuclear spin interaction. We discuss the method for calculating the Hamiltonian matrix in the chosen basis.

Then, we consider the effect of an external static magnetic field, leading to the Zeeman Hamiltonian. This interaction further splits the energy levels and is crucial for understanding the behavior of the molecule under laboratory conditions.

Finally, we present the calculation of eigenstates at zero field and in the presence

of a magnetic field, providing a complete picture of the hyperfine structure and its dependence on external influences.

2.1 The angular momentum coupling scheme

Each particle has a spin and a orbital angular momentum. In this case we consider the total spin of the two hydrogen nuclei $\mathbf{I} = \mathbf{I_1} + \mathbf{I_2}$. Since these are both protons, we have for each nuclear spin $I_i = \frac{1}{2}$ $(i = 1, 2)$. This coupled quantity is chosen, since the two nuclei are identical and thus they cannot be distinguished, by the symmetry of the molecule. The quantum number I can, as the tensor product of two spin $\frac{1}{2}$ particles, only take the values 1 (triplet states) or 0 (singlet state). We call the nuclear spin vector space V_I. The electron is a spin $\frac{1}{2}$ particle, we call its spin $\mathbf{S_e}$ and the electron spin vector space V_S. For the orbital angular momenta, we choose to consider the total orbital angular momentum $\mathbf{L}$ $(= \mathbf{L_1} + \mathbf{L_2} + \mathbf{L_e})$, which can take on any integer value and call the vector space V_L. We do this, as the eigenstates of the non-relativistic Hamiltonian are ordered by this number (and the vibrational level ν).

The total angular momentum vector space is the tensor product $V_L \bigotimes V_S \bigotimes V_I$. The order in which the three spaces lie in this product does in principle not matter, but the same order has to be followed consistently throughout the entire analysis. We choose this order here and follow it through the next sections. This vectorspace has the basis $|L, m_L; S_e, m_S; I, m_I\rangle = |L, m_L\rangle \otimes |S_e, m_S\rangle \otimes |I, m_I\rangle$, where in each space the respective basis obeys its respective angular momentum basis equations A.1.

This is a valid choice for the basis, but one tries to find a basis in which the Hamiltonian is as close to diagonal as possible. For practical purposes, we will not use this basis, as the eigenstates of the Hamiltonian differ significantly from them. For this reason, new quantum numbers are defined as coupled angular momenta. It turns out that the Hamiltonian is nearly diagonal for the coupled angular momentum basis, at least with no external fields present.

First the total spin $\mathbf{F} = \mathbf{S_e} + \mathbf{I}$ is defined, it has the vectorspace $V_F = V_S \bigotimes V_I$ and following equation A.3, the total space $V_L \bigotimes V_F$ has the coupled basis $|L, m_L; (S_e, I)F, m_F\rangle$. As a last step, we couple the two reminding angular momenta to one total angular momentum $\mathbf{J} = \mathbf{L} + \mathbf{F}$ with the coupled basis $|(L, (S_e, I)F); J, M_J\rangle$. This is the basis that is used when dealing with the hyperfine structure of this molecule.

From the non-relativistic Hamiltonian H_0 for the Σ_g band (the same goes for the Σ_u band) one finds energy states, which are labeled by their ro-vibrational level

(ν, L). When talking about hyperfine states in this analysis if nothing else is stated, the Σ_g sideband is assumed, since all the bond states, except for four weakly bound Σ_u states, are in this band.

When we consider the ro-vibrational level (ν, L), since for even L for parity reasons the nuclear spin has to be $I = 0$ and for odd L the nuclear spin is $I = 1$ for all the states within the band (the other way around in Σ_u), the number I is omitted when writing the basis, as it is completely determined by L. Since the spin of the electron is always $S_e = \frac{1}{2}$, this letter is omitted in the basis as well. For that reason, when considering a ro-vibrational level (ν, L) the coupled basis states discussed above will just be labeled $|F, J, M_J\rangle$.

2.2 The effective spin Hamiltonian

The leading correction to the non-relativistic energy is determined by the so called Breit-Pauli Hamiltonian, it gives the relativistic correction up to the order α^2, where α is the fine structure constant, as the QED corrections are expanded in a series of powers of this constant. In [5] it is shown that one can express this interaction in terms of an effective spin Hamiltonian, that consists of five terms:

$$\begin{aligned} H_{hf} = {} & b_F(\mathbf{I}\cdot\mathbf{S_e}) + c_e(\mathbf{L}\cdot\mathbf{S_e}) + c_I(\mathbf{L}\cdot\mathbf{I}) \\ & + \frac{d_1}{(2L-1)(2L+3)}\left(\frac{2}{3}\mathbf{L}^2(\mathbf{I}\cdot\mathbf{S_e}) - \{(\mathbf{L}\cdot\mathbf{I}),(\mathbf{L}\cdot\mathbf{S_e})\}\right) \\ & + \frac{d_2}{(2L-1)(2L+3)}\left(\frac{1}{3}\mathbf{L}^2\mathbf{I}^2 - \frac{1}{2}(\mathbf{L}\cdot\mathbf{I}) - (\mathbf{L}\cdot\mathbf{I})^2\right), \end{aligned} \tag{2.1}$$

Where the different coupling constants $(b_F, c_e, c_I, d_1, d_2)$ are determined numerically and depend on the ro-vibrational level (ν, L) of the molecule. These constants were first calculated in table I in [5] for the lowest ro-vibrational states ($0 \le \nu \le 4$ and $0 \le L \le 4$) up relative theoretical accuracy of $O(\alpha^2)$.

In the case of ortho-H_2^+, meaning when L is odd (in the Σ_g band), the spin-spin electron-proton interaction is the strongest. For that reason, accuracy in the coupling coefficient b_F is of utmost importance. Over the years different papers have provided improved values for some levels. A $m\alpha^6(m/M)$ correction term is treated first in [9] and then to full extend, with higher-order QED corrections in [10] (for $L = 1, 3$ and $0 \le v \le 10$). Some higher-order corrections to spin-orbit and spin-spin tensor interactions made in [11] led to more accurate c_e and d_1 coefficients.

To actually compute the matrix elements of this Hamiltonian here we have split

the five parts and calculated each separately, which is a simpler problem. This way it was easier to spot mistakes and compare the results with the ones stated in the literature.

$$H_{hf} = b_F H_1 + c_e H_2 + c_I H_3 + \frac{d_1}{(2L-1)(2L+3)} H_4 + \frac{d_2}{(2L-1)(2L+3)} H_5, \qquad (2.2)$$

In [6] formulas are given for each of the matrix elements of the effective spin Hamiltonian. These are obtained by doing the calculations as in the following subsection and then setting in the actual values for (F, J, M_J) and (F', J', M'_J) in the formulas found. Our results found here match these equations.

2.2.1 Matrix elements

This interaction is composed by many different rank 0 tensor operators acting on the various subspaces of the composed spin tensor space $V_L \bigotimes V_S \bigotimes V_I$. In this subsection we will calculate the matrix elements of the different operators in the coupled basis $|F, J, M_J\rangle$. Since the operators are of rank 0, we know that the Hamiltonian will be diagonal in both J and M_J due to the Wigner-Eckart theorem A.9.

$$\begin{aligned} \langle F, J, M_J | \, T_0^{(0)} \, | F', J', M'_J \rangle &= \frac{1}{\sqrt{(2J+1)}} C^{J,M}_{J',M';0,0} \, \langle F, J || \mathbf{T}^{(0)} || F', J' \rangle \\ &= \frac{1}{\sqrt{(2J+1)}} \delta_{J,J'} \delta_{M_J,M'_J} \, \langle F, J || \mathbf{T}^{(0)} || F, J \rangle \, , \end{aligned} \qquad (2.3)$$

Here we have used the notation for the Clebsch-Gordan coefficients as in the appendix, where $C^{J,M_J}_{j_1,m_1;j_2,m_2} = \langle j_1, m_1; j_2, m_2 | J, M_J \rangle$. This already limits the possible non-zero off-diagonal terms to those where only the total spin of the two states is different ($F \neq F'$), but the other quantum numbers are equal. The next step in our analysis is to calculate matrix elements involving each of the operators in H_{hf} concretely.

First we consider the spin-spin interaction operator $(\mathbf{I} \cdot \mathbf{S_e})$. The question is how does one compute matrix elements in the basis $|F, J, M_J\rangle$. One way would be to use the strategies developed in the Appendix A involving reduced matrix elements. For this operator, there happens to be a more simple way to solve the problem, since $\mathbf{I}$ and $\mathbf{S_e}$ commute.

$$\mathbf{F}^2 = \mathbf{I}^2 + 2(\mathbf{I}\cdot\mathbf{S_e}) + {\mathbf{S_e}}^2, \tag{2.4}$$

Knowing that one can calculate the matrix element, by writing it in terms of operators, with respect to which the basis states are eigenstates of.

$$\begin{aligned}\langle F, J, M_J|(\mathbf{I}\cdot\mathbf{S_e})|F', J', M_J'\rangle &= \langle F, J, M_J|\frac{1}{2}(\mathbf{F}^2 - \mathbf{I}^2 - {\mathbf{S_e}}^2)|F', J', M_J'\rangle \\ &= \frac{1}{2}\left(F'(F'+1) - I'(I'+1) - S_e'(S_e'+1)\right) \\ &\quad \times \langle F, J, M_J|F', J', M_J'\rangle \\ &= \frac{1}{2}\left(F(F+1) - I(I+1) - S_e(S_e+1)\right) \\ &\quad \times \delta_{FF'}\delta_{JJ'}\delta_{M_J M_J'},\end{aligned} \tag{2.5}$$

In the next step we calculate the matrix elements involving spin-rotation coupling operators $(\mathbf{L}\cdot\mathbf{S_e})$ and $(\mathbf{L}\cdot\mathbf{I})$. For this calculation we will need the strategies developed in the Appendix A. Both these operators are of the shape $(\mathbf{L}^{(1)}\otimes\mathbf{T}_F^{(1)})^{(0)}$ in the space $V_L \bigotimes V_F$, where $\mathbf{T}_F^{(1)}(=\mathbf{S_e}, \mathbf{I})$ is a rank 1 tensor operator in the space V_F. For reduced matrix elements involving these operators we can use equation A.15 to calculate the reduced matrix element.

$$\begin{aligned}\langle F, J||(\mathbf{L}\cdot\mathbf{T_F})||F', J\rangle = \sqrt{(2J+1)}(-1)^{J+L'+F}&\begin{Bmatrix} L & 1 & L' \\ F' & J & F\end{Bmatrix} \\ &\times \langle L||\mathbf{L}||L'\rangle \langle F||\mathbf{T_F}||F'\rangle,\end{aligned} \tag{2.6}$$

In this expression a Wigner-6-j symbol is used in the curved brackets, as introduced in the appendix, in equation A.7. To calculate the reduced matrix elements on the V_F space now, we use equation A.13 for $\mathbf{T}_F^{(1)} = ({\mathbf{S_e}}^{(1)}\otimes\mathbb{1})^{(1)}$ and equation A.14 for $\mathbf{T}_F^{(1)} = (\mathbb{1}\otimes\mathbf{I}^{(1)})^{(1)}$. We obtain the expressions:

$$\begin{aligned}\langle F||\mathbf{S_e}||F'\rangle &= (-1)^{F+I+S_e'+1}\sqrt{(2F+1)(2F'+1)}\begin{Bmatrix} S_e & 1 & S_e' \\ F' & I & F\end{Bmatrix}\langle S_e||\mathbf{S_e}||S_e'\rangle\,\delta_{I,I'}, \\ \langle F||\mathbf{I}||F'\rangle &= (-1)^{F'+I+S_e+1}\sqrt{(2F+1)(2F'+1)}\begin{Bmatrix} I & 1 & I' \\ F' & S_e & F\end{Bmatrix}\langle I||\mathbf{I}||I'\rangle\,\delta_{S_e S_e'},\end{aligned} \tag{2.7}$$

The last reduced matrix elements can simply be calculated using the equation A.12 for the three cases L, S_e and I. The full expression is obtained by putting the equations above together. For the two operators we find:

$$\begin{aligned}\langle F, J, M_J|(\mathbf{L}\cdot\mathbf{S_e})|F', J', M_J'\rangle = \delta_{JJ'}\delta_{M_J M_J'}\delta_{LL'} \begin{Bmatrix} L & 1 & L \\ F' & J & F \end{Bmatrix} \begin{Bmatrix} S_e & 1 & S_e \\ F' & I & F \end{Bmatrix} \\ \times (-1)^{J+L+F+F'+I+S_e+1}\sqrt{(2F+1)(2F'+1)} \\ \times \sqrt{L(L+1)(2L+1)}\sqrt{S_e(S_e+1)(2S_e+1)},\end{aligned} \tag{2.8}$$

$$\begin{aligned}\langle F, J, M_J|(\mathbf{L}\cdot\mathbf{I})|F', J', M_J'\rangle = \delta_{JJ'}\delta_{M_J M_J'}\delta_{LL'} \begin{Bmatrix} L & 1 & L \\ F' & J & F \end{Bmatrix} \begin{Bmatrix} I & 1 & I \\ F' & S_e & F \end{Bmatrix} \\ \times (-1)^{J+L+F+F+I+S_e+1}\sqrt{(2F+1)(2F'+1)} \\ \times \sqrt{L(L+1)(2L+1)}\sqrt{I(I+1)(2I+1)},\end{aligned} \tag{2.9}$$

Although the expressions look very similar, there are small, but important differences, such as having a F' instead of a F in the phase. The matrix elements of products of such operators like $(\mathbf{L}\cdot\mathbf{I})(\mathbf{L}\cdot\mathbf{I})$ can be calculated by multiplying the two individual matrixes meaning, we have to sum over all the different hyperfine states. If we have in general two rank 0 operators $\mathbf{T}^{(0)}$ and $\tilde{\mathbf{T}}^{(0)}$, then we can write the matrix element of the product as:

$$\begin{aligned}\langle F, J, M_J|\,\mathbf{T}^{(0)}\tilde{\mathbf{T}}^{(0)}\,|F', J', M_J'\rangle = \sum_{F'', J'', M_J''} \langle F, J, M_J|\mathbf{T}^{(0)}\,|F'', J'', M_J''\rangle \\ \times \langle F'', J'', M_J''|\tilde{\mathbf{T}}^{(0)}\,|F', J', M_J'\rangle\,,\end{aligned} \tag{2.10}$$

The last kind of operators that appear in the effective spin Hamiltonian are $\mathbf{L}^2$ and $\mathbf{I}^2$. Matrix elements involving these operators can be calculated, by making use that the basis states are eigenstates of these operators, of eigenvalues $L(L+1)$ and $I(I+1)$ respectively.

With that we have described how to calculate matrix elements involving all the operators that appear in the effective Hamiltonian H_{hf} and we can calculate the full matrix as a sum of expressions of that shape.

2.2.2 Para-H_2^+

For para-H_2^+, meaning the nuclear spin is in the singlet state $I = 0$, most of the terms in the Hamiltonian vanish. For the bond states, this is the case for all even orbital angular momentum states L. In fact we can write the Hamiltonian in this case as just:

$$H_{hf} = c_e(\mathbf{L} \cdot \mathbf{S_e}), \tag{2.11}$$

From equation 2.8 we cannot directly see, that the Hamiltonian is diagonal in the $|F, J, M_J\rangle$ basis. This is true, because in this case the total spin quantum number is the same as the electron spin $F = S_e = \frac{1}{2}$. As there is only one possible F, the Hamiltonian is diagonal in the coupled basis, splitting the states into two different energies, according to $J = L \pm \frac{1}{2}$.

Another interesting property is that in general, for all Para states, the c_e coefficients are small compared to the dominating b_F coefficients, that we have for ortho-H_2^+. For that reason the hyperfine energy shift is much smaller than for ortho-H_2^+. For the para-groundstate $(\nu, L) = (0, 0)$ there is no hyperfine splitting. Because of that, we have calculated the energies for the first excited rotational level $(\nu, L) = (0, 2)$ in table 2.1.

2.2.3 Ortho-H_2^+

For ortho-H_2^+, where the nuclear spin is in the triplet state with $I = 1$, the effective spin Hamiltonian is composed by the five components as stated in equation 2.1. The strength of each of the five contributions is encoded in the coupling coefficients. The largest coefficient for all levels, as mentioned above, is b_F. This corresponds to the term that is diagonal in the coupled basis. Thus, the entries on the diagonal will in general be much larger than the off-diagonal terms, and the coupled basis $|F, J, M_J\rangle$ is close to the eigenbasis of this Hamiltonian.

For these levels, this Hamiltonian splits the states into five levels for $L = 1$ and six for all other odd L. The possible quantum numbers (F, J) for these levels are $F \in \{\frac{1}{2}, \frac{3}{2}\}$ and $J \in \{L + F, ..., |L - F|\}$. For this reason, these levels have a much richer hyperfine structure than the para counterpart. One can see this in table 2.1, where the energies of this Hamiltonian have been computed for the Ortho-groundstate $(\nu, L) = (0, 1)$ comparing it to a Para state.

Para State: Ro-vibrational Level $(\nu, L) = (0, 2)$	
State $\lvert F, J\rangle$	**Energy (MHz)**
$\lvert\frac{1}{2}, \frac{1}{2}\rangle$	-63.24527149
$\lvert\frac{1}{2}, \frac{3}{2}\rangle$	42.16350586
Ortho State: Ro-vibrational Level $(\nu, L) = (0, 1)$	
State $\lvert\tilde{F}, J\rangle$	**Energy (MHz)**
$\lvert\frac{1}{2}, \frac{1}{2}\rangle$	-910.696074
$\lvert\frac{1}{2}, \frac{3}{2}\rangle$	-930.371709
$\lvert\frac{3}{2}, \frac{1}{2}\rangle$	385.366110
$\lvert\frac{3}{2}, \frac{3}{2}\rangle$	481.923026
$\lvert\frac{3}{2}, \frac{5}{2}\rangle$	474.075770

Table 2.1: Hyperfine energy levels for two para and ortho levels of H_2^+. One can clearly see that the hyperfine splitting is much larger for ortho-H_2^+. For para-H_2^+ the eigenstates are $|F, J\rangle$, whereas for ortho-H_2^+ the states are $|\tilde{F}, J\rangle$, where the $\tilde{F}$ is introduced in equation 2.24.

2.3 Interaction with a Static Magnetic Field

Magnetic moments arise in systems of charged particles with nonzero angular momenta, to which they are proportional. The magnetic dipole moment of an object determines the magnitude of the torque the object experiences in a given magnetic field. The magnetic dipole moment of an electron (proton) with spin S_e (I_p) and orbital angular momentum L_e (L_p) can be expressed as:

$$\mu_{\mathbf{e}} = -g_e \mu_B \mathbf{S_e} - \mu_B \mathbf{L_e}, \tag{2.12}$$

$$\mu_{\mathbf{p}} = g_N \mu_N \mathbf{I_p} + \mu_N \mathbf{L_p}, \tag{2.13}$$

where g_e is the electron g-factor, g_N is the nucleus g-factor, μ_B is the Bohr magneton, and μ_N is the nuclear magneton. The different signs arise from the opposite charges of the particles. We can define the magnetic dipole moment of the H_2^+ molecular ion, a system consisting of one electron and two protons, as the sum of three such operators. It can be written as a tensor operator of rank 1, which can be written in cyclic components.

$$\mu^{(1)} = -g_e \mu_B \mathbf{S_e}^{(1)} + g_N \mu_N \mathbf{I}^{(1)} + \mu_N \left(\mathbf{L_1} + \mathbf{L_2}\right)^{(1)} - \mu_B \mathbf{L_e}^{(1)}, \tag{2.14}$$

We can write this expression in a way to make clear on which angular momentum subspace of $V_L \bigotimes V_S \bigotimes V_I$ each operator acts on. Written this way the expression becomes:

$$\begin{aligned} \mu^{(1)} = &-g_e \mu_B (\mathbb{1} \otimes \mathbb{1} \otimes \mathbf{S_e}^{(1)})^{(1)} + g_N \mu_N (\mathbb{1} \otimes \mathbf{I}^{(1)} \otimes \mathbb{1})^{(1)} \\ &- \mu_B \left([\mathbf{L_e} - \frac{m_e}{m_p} (\mathbf{L_1} + \mathbf{L_2})]^{(1)} \otimes \mathbb{1} \otimes \mathbb{1} \right)^{(1)}, \end{aligned} \tag{2.15}$$

In this equation, we used that $\frac{\mu_N}{\mu_B} = \frac{m_e}{m_p}$. For clarity and spacing reasons, the matrix elements of the magnetic dipole operator are computed in three parts. The first term corresponds to the electron spin, the second to the nuclear spin, and the third to the orbital angular momentum. With equations A.13 and A.14, we find on the tensor space $V_J = V_L \bigotimes V_F$:

$$\langle J||\mathbf{T_L}||J'\rangle = (-1)^{J'+L+F+1}\sqrt{(2J+1)(2J'+1)}\begin{Bmatrix} L & 1 & L \\ J' & F & J \end{Bmatrix}\langle L||\mathbf{T_L}||L\rangle\,\delta_{FF'},$$
$$\langle J||\mathbf{T_F}||J'\rangle = (-1)^{J+L+F'+1}\sqrt{(2J+1)(2J'+1)}\begin{Bmatrix} F & 1 & F' \\ J' & L & J \end{Bmatrix}\langle F||\mathbf{T_F}||F'\rangle\,\delta_{LL'}, \tag{2.16}$$

where the two equations hold for any rank 1 tensor $\mathbf{T_L}^{(1)}$ ($\mathbf{T_F}^{(1)}$) acting only on one subspace V_L (V_F), which is the case for all the operators considered. The same can be done for the tensor space $V_F = V_I \bigotimes V_S$, and we find again the two equations 2.7.

With knowledge of equations 2.16 and 2.7, we can calculate each part of the magnetic dipole operator $\mu_q^{(1)}$. The matrix elements for the two spin terms, electron $\mathbf{S_e}$ and nuclear $\mathbf{I}$, can be expressed as:

$$\begin{aligned}\langle F, J, M_J|\,(\mathbf{S_e})_q^{(1)}\,|F', J', M_J'\rangle &= C^{J,M_J}_{J',M_J';1,q}(-1)^{J+L+F'+F'+S_e+I}\sqrt{(2J'+1)} \\ &\times \begin{Bmatrix} F & 1 & F' \\ J' & L & J \end{Bmatrix}\begin{Bmatrix} S_e & 1 & S_e \\ F' & I & F \end{Bmatrix} \\ &\times \sqrt{(2F+1)(2F'+1)}\sqrt{S_e(S_e+1)(2S_e+1)}, \\ \langle F, J, M_J|\,(\mathbf{I})_q^{(1)}\,|F', J', M_J'\rangle &= C^{J,M_J}_{J',M_J';1,q}(-1)^{J+L+F'+F+S_e+I}\sqrt{(2J'+1)} \\ &\times \begin{Bmatrix} F & 1 & F' \\ J' & L & J \end{Bmatrix}\begin{Bmatrix} I & 1 & I \\ F' & S_e & F \end{Bmatrix} \\ &\times \sqrt{(2F+1)(2F'+1)}\sqrt{I(I+1)(2I+1)},\end{aligned} \tag{2.17}$$

The orbital angular momentum term is not as straightforward to calculate. The three operators that appear are $\mathbf{L_1}$, $\mathbf{L_2}$ and $\mathbf{L_e}$, which by the first equation in 2.16 lead to reduced matrix elements $\langle L||\mathbf{L_i}^{(1)}||L\rangle$ (for $i = 1, 2, e$). These depend on the orbital wavefunction of the ro-vibrational level (ν, L), which is obtained from the non-relativistic Hamiltonian and thus have to be calculated numerically. This calculation has been performed in [7] for all levels with $0 \leq \nu \leq 4$ and $0 \leq L \leq 4$. To abbreviate the equations, in this paper a new operator $\mathbf{L_{tot}}$ is defined, which describes all the orbital angular momentum dependence.

$$\mathbf{L_{tot}} = \frac{1}{\sqrt{2L+1}} \left(\mathbf{L_e} - \frac{m_e}{m_p}(\mathbf{L_1} + \mathbf{L_2}) \right), \tag{2.18}$$

This operator leads to the reduced matrix element $\langle ||\mathbf{L_{tot}}|| \rangle$. Using the symmetry of H_2^+ under the exchange of the two nuclei, it follows that for the reduced matrix elements one has:

$$\langle \nu, L| \, |L_1| \, |\nu, L\rangle = \langle \nu, L| \, |L_2| \, |\nu, L\rangle \, , \tag{2.19}$$

And the reduced matrix element of this new operator can be expressed as:

$$\langle ||\mathbf{L_{tot}}|| \rangle = \frac{\langle \nu, L| \, |L_e| \, |\nu, L\rangle}{\sqrt{2L+1}} - 2\frac{m_e}{m_p}\frac{\langle \nu, L| \, |L_1| \, |\nu, L\rangle}{\sqrt{2L+1}}, \tag{2.20}$$

The reduced matrix elements $\langle ||\mathbf{L_{tot}}|| \rangle$ are given for all ro-vibrational states with $0 \leq \nu \leq 4$ and $0 \leq L \leq 4$ in [7]. With this reduced matrix element $\langle ||\mathbf{L_{tot}}|| \rangle$, we can write the orbital angular momentum term of the magnetic dipole operator as:

$$\begin{aligned} \langle F, J, M_J| \, (\mathbf{L_{tot}})^{(1)}_q \, |F', J', M'_J\rangle = C^{J,M_J}_{J',M'_J;1,q}(-1)^{J'+L+F+1}\sqrt{(2J'+1)} \\ \times \begin{Bmatrix} L & 1 & L \\ J' & F & J \end{Bmatrix} \sqrt{(2L+1)} \, \langle ||\mathbf{L_{tot}}|| \rangle \, \delta_{FF'}, \end{aligned} \tag{2.21}$$

2.3.1 The Zeeman Hamiltonian

The interaction of a magnetic moment with a static magnetic field is described by the Zeeman Hamiltonian. This Hamiltonian is crucial for understanding how magnetic fields affect atomic and molecular systems, particularly in the context of spectroscopy and magnetic resonance. For a static magnetic field $\mathbf{B}$, the Zeeman Hamiltonian is expressed as:

$$H_Z = -(\mu \cdot \mathbf{B}), \tag{2.22}$$

In this equation, $\mathbf{B} = (B_{+1}, B_0, B_{-1})$ is treated as a rank 1 tensor in cyclic components. The magnetic field is assumed to be directed along the quantization axis ($\mathbf{B} = B \cdot \hat{e_z}$), implying $\mathbf{B}^{(1)} = B_0^{(1)}$. The Hamiltonian can thus be expressed as a sum of several terms, each involving the zeroth component of a rank 1 irreducible

tensor operator, which acts on one of the three spaces in $V_L \bigotimes V_I \bigotimes V_S$ of angular momentum.

$$\begin{aligned} H_Z &= -\mu_0^{(1)} B \\ &= g_e \mu_B B (\mathbb{1} \otimes \mathbb{1} \otimes \mathbf{S_e}^{(1)})_0^{(1)} - g_N \mu_N B (\mathbb{1} \otimes \mathbf{I}^{(1)} \otimes \mathbb{1})_0^{(1)} \\ &\quad + \mu_B B \frac{1}{\sqrt{2L+1}} (\mathbf{L_{tot}}^{(1)} \otimes \mathbb{1} \otimes \mathbb{1})_0^{(1)}, \end{aligned} \tag{2.23}$$

This formulation indicates that the case $q = 0$ is considered for the matrix elements of the Hamiltonian, as given in equations 2.17 and 2.21. Notably, this operator is not diagonal in the basis $|F, J, M_J\rangle$, meaning that as the magnetic field increases, the states become more mixed. However, due to the presence of only the $q = 0$ component of the tensors, there is no mixing between states with different total angular momentum projection M_J, so the mixing is limited to those states with the same projection. Interestingly this Hamiltonian is indeed diagonal for the uncoupled basis $|L, m_L; S_e, m_S; I, m_I\rangle$.

Previous studies, such as [7], have considered two special cases where the interaction can be treated as approximately linear. In the weak field regime, the Zeeman effect is treated as a perturbation, and only the diagonal terms of H_Z in the coupled basis $|F, J, M_J\rangle$ (also in the eigenbasis $|\tilde{F}, J, M_J\rangle$ of H_{hf}) are considered. The other case is the strong field regime (Paschen–Back effect), where the external magnetic field is sufficiently strong to disrupt the coupling between orbital ($\mathbf{L}$) and spin ($\mathbf{S_e}$, $\mathbf{I}$) angular momenta. So H_Z is treated exactly in the basis $|L, m_L; S_e, m_S; I, m_I\rangle$ as a diagonal matrix and the Hamiltonian H_{hf} is treated as a perturbation and only its diagonal terms in this basis are considered.

In both cases, the g-factors of the interaction are obtained, leading to a linear shift in the hyperfine energy levels. Here the Zeeman effect is not treated perturbatively but exactly. This approach allows recovery of the special cases computed in [7] by considering the limits of very small or very large fields B. Additionally it allows one to examine the region where the magnetic field is of intermediate strength, meaning the Hamiltonians H_{hf} and H_z are comparable and due to the state mixing, the shift of the eigenenergies can be highly nonlinear.

2.4 Eigenstates

In the previous section, the focus was on computing the matrix elements of the two different Hamiltonians that are responsible for the hyperfine splitting of the ro-vibrational levels of H_2^+. Once the matrices are calculated, they can be diagonalized, yielding the eigenstates with their eigenenergies for this interaction.

2.4.1 At zero field

If there is no magnetic field, the hyperfine splitting is given by the interaction of the effective spin Hamiltonian $H_{eff} = H_{hf}$. As seen in the previous subsection, this Hamiltonian is diagonal in J as well as in M_J, but there are some off diagonal terms for different total spins ($F \neq F'$) in ortho-H_2^+. This means that the chosen basis $|F, J, M_J\rangle$ is not an eigenbasis of the Hamiltonian.

In [7] this is solved by introducing the eigenbasis $|\tilde{F}, J, M_J\rangle$, where this new number $\tilde{F}$ takes into account the state mixing. We have thus the basis states:

$$|\tilde{F}, J, M_J\rangle = C_1^{\pm} \, |\frac{1}{2}, J, M_J\rangle + C_3^{\pm} \, |\frac{3}{2}, J, M_J\rangle \,, \tag{2.24}$$

This $\tilde{F}$ take on the same values as F, the upper index ($\pm$) in the coefficients $[C_1^{\pm}, C_3^{\pm}]$ correspond to $\tilde{F} = \frac{1}{2}$ for the upper index ($-$) and to $\tilde{F} = \frac{3}{2}$ for the upper index ($+$). For all the ro-vibrational levels this mixing is small, amounting to less than 1% (meaning $\left|C_1^-\right|^2, \left|C_3^+\right|^2 \approx 1$). This is the reason, why F is still relatively a good quantum number.

2.4.2 For a magnetic field B

Now we consider the case, where there is a nonzero, static magnetic field B. The Hamiltonian matrix considered for the hyperfine splitting now is $H_{eff} = H_{hf} + H_Z$. We calculate this matrix following the steps above in the $|F, J, M_J\rangle$ basis. Now we can obtain for each ro-vibrational level (ν, L) at each magnetic field strength B an eigenbasis of the Hamiltonian, by diagonalizing the matrix. We need to introduce a more general notation for the eigenstates than in the zero field case:

$$|i(B)\rangle = \sum_{F,J} \quad c^{(i)}_{F,J,M_J}(B) \quad |F, J, M_J\rangle \,, \tag{2.25}$$

Where $c^{(i)}_{F,J,M_J}(B)$ are the magnetic field dependent coefficients of the coupled basis state $|F, J, M_J\rangle$ in the eigenstate of the Hamiltonian $|i(B)\rangle$. Often we will omit

the argument B, if it is clear which field we have. No sum over the different M_J is necessary, as there is no state mixing between these states in neither of the interactions. This leads to the existence of so called stretched states, which are those with maximal (or minimal) total angular momentum projection. For para-H_2^+ we have the stretched states $|F = \frac{1}{2}, J = L + \frac{1}{2}, M_J = \pm(L + \frac{1}{2})\rangle$, and for ortho-$H_2^+$ we have $|F = \frac{3}{2}, J = L + \frac{3}{2}, M_J = \pm(L + \frac{3}{2})\rangle$. As there is only one possible state with that projection, $M_J = \pm(L+\frac{1}{2})$ for para, and $M_J = \pm(L+\frac{3}{2})$ for ortho; stretched states are always pure states of the Hamiltonian and are therefore of special importance.

One way to order and label the states would be by ordering them by their energy. The problem with this scheme is that as the magnetic field changes, some levels may cross and thus different states would be labeled as the i-th state depending on the magnetic field strength.

Here we choose the labeling in the following way. If we consider the zero field, the labels are $|i(0)\rangle = |\tilde{F}, J, M_J\rangle$ such that the order of i is increasing first in F, then in J and last in M_J. This is displayed explicitly for the four lowest rotational levels in the Appendix B. Thus the i-th state $|i(B)\rangle$ will be the eigenstate at magnetic field B, to which $|i(0)\rangle$ evolves when increasing the magnetic field. Thus when plotting the eigenstates against the magnetic field B, each eigenstate $|i(B)\rangle$ is represented by a smooth line. This is for example displayed in the plot 2.1 for the ro-vibrational level $(3, 2)$.

Often for a given magnetic field B the eigenstates $|i(B)\rangle$ will be referred to as $|F, J, M_J\rangle$. This does not mean that we are considering that pure state, but the state which evolves as stated above. Additionally for the magnetic fields considered and the given ro-vibrational levels, the state mixing is relatively small, such that it still makes sense to use this labeling. As an example in table 2.2 the eigenstates of the ortho-groundstate at the magnetic field $B = 450\mu$T have been calculated, together with their coefficient corresponding to the pure state.

This labeling scheme is useful for smaller magnetic fields, as the ones considered here. If we were to only work near the Paschen-Back regime, it would be better to choose the labeling according to the uncoupled $|L, m_L; S_e, m_S; I, m_I\rangle$, that the states evolve into for large B.

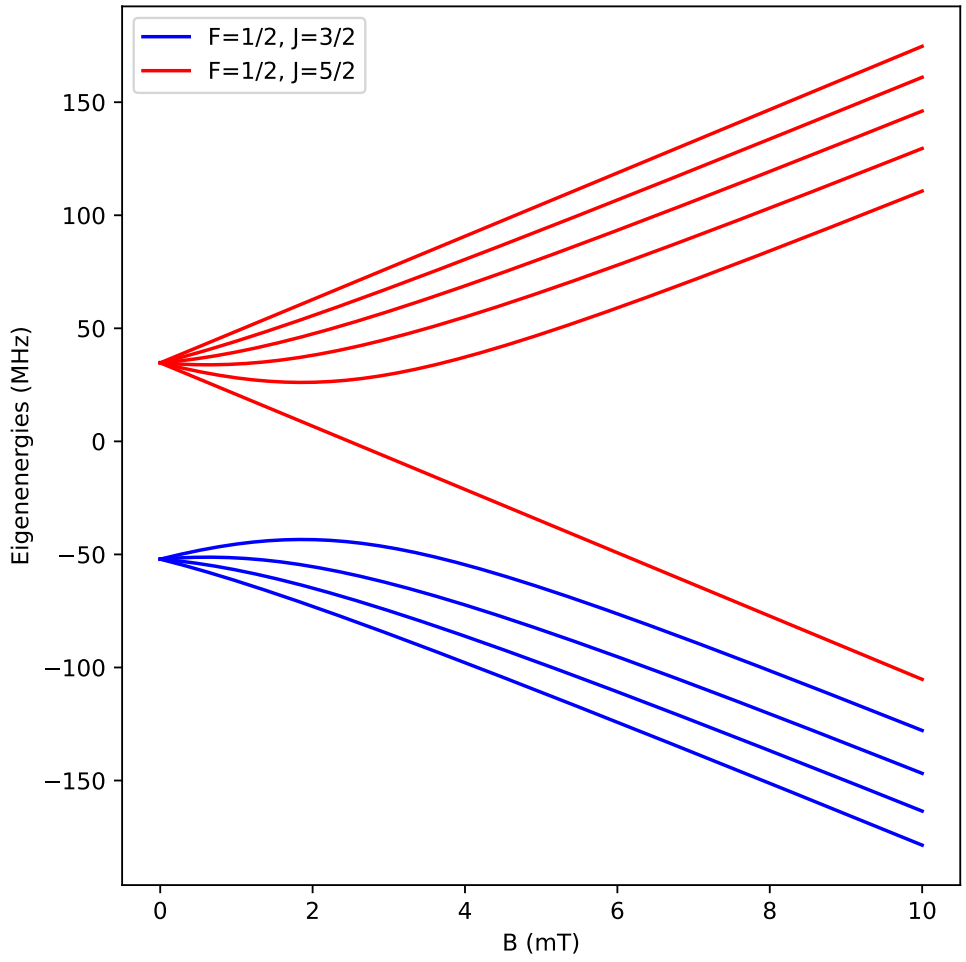

Figure 2.1: The magnetic-field-dependent hyperfine structure of the $(\nu, L) = (3, 2)$ ro-vibrational level in the 0-10 mT range. We can clearly distinguish three regions. At zero field, the levels are split in two according to the coupled basis (F, J), with $F = \frac{1}{2}$ and $J = (2 \pm \frac{1}{2})$. In the weak-field (Zeeman) regime (0-1 mT) the states follow a linear behaviour, with tangents according to the projection M_J. Then many states follow curves which are highly nonlinear (1-6 mT). For large magnetic fields, the hyperfine Paschen-Back regime, all the lines are again straight (6-10 mT). On the right, at 10 mT, we see the levels split according to the uncoupled basis $|L, m_L; S_e, m_S\rangle$. We have a large split according to $m_S = \pm\frac{1}{2}$ and then a finer split within that, according to m_L.

$(\nu, L) = (0, 1)$				B=450.0 [μT]	
i	F	J	M_J	Energy [MHz]	$\lvert c^{(i)}_{F,J,M_J}(B)\rvert^2$
0	$\frac{1}{2}$	$\frac{1}{2}$	$-\frac{1}{2}$	-910.91311	0.98775
1	$\frac{1}{2}$	$\frac{1}{2}$	$+\frac{1}{2}$	-910.13871	0.98951
2	$\frac{1}{2}$	$\frac{3}{2}$	$-\frac{3}{2}$	-928.16289	0.99982
3	$\frac{1}{2}$	$\frac{3}{2}$	$-\frac{1}{2}$	-929.86044	0.9888
4	$\frac{1}{2}$	$\frac{3}{2}$	$+\frac{1}{2}$	-931.32705	0.99097
5	$\frac{1}{2}$	$\frac{3}{2}$	$+\frac{3}{2}$	-932.6302	0.99966
6	$\frac{3}{2}$	$\frac{1}{2}$	$-\frac{1}{2}$	381.49087	0.99779
7	$\frac{3}{2}$	$\frac{1}{2}$	$+\frac{1}{2}$	389.08379	0.99726
8	$\frac{3}{2}$	$\frac{3}{2}$	$-\frac{3}{2}$	477.74376	0.93252
9	$\frac{3}{2}$	$\frac{3}{2}$	$-\frac{1}{2}$	481.16472	0.92035
10	$\frac{3}{2}$	$\frac{3}{2}$	$+\frac{1}{2}$	484.2651	0.93007
11	$\frac{3}{2}$	$\frac{3}{2}$	$+\frac{3}{2}$	487.07844	0.95601
12	$\frac{3}{2}$	$\frac{5}{2}$	$-\frac{5}{2}$	467.79247	1
13	$\frac{3}{2}$	$\frac{5}{2}$	$-\frac{3}{2}$	469.78524	0.93265
14	$\frac{3}{2}$	$\frac{5}{2}$	$-\frac{1}{2}$	472.1318	0.92134
15	$\frac{3}{2}$	$\frac{5}{2}$	$+\frac{1}{2}$	474.6973	0.93119
16	$\frac{3}{2}$	$\frac{5}{2}$	$+\frac{3}{2}$	477.43984	0.95629
17	$\frac{3}{2}$	$\frac{5}{2}$	$+\frac{5}{2}$	480.35907	1

Table 2.2: The hyperfine eigenstates of the ortho-groundstate $(\nu, L) = (0, 1)$ at a magnetic field of 450 μT. The state index i as well as the corresponding quantum numbers (F, J, M_J) are displayed, together with the hyperfine energy shift and the coefficient corresponding to the pure state with these quantum numbers. The state mixing in this case is maximal for the state 9, at almost 8%. The only pure states are the two stretched states.

Figure 2.2: Schematic representation of the hyperfine states of the ortho-groundstate $(\nu, L) = (0, 1)$ at 450 μT. Colors represent different (F, J) quantum numbers, with corresponding hyperfine energy levels labeled in MHz. Horizontal positions indicate different M_J values, ranging from left (negative) to right (positive). Note that these states are the eigenstates of the Hamiltonian rather than the pure $|F, J, M_J\rangle$ states. The figure is illustrative and not to scale.

Chapter 3

The hyperfine structure of $^9Be^+$

In experimental setups such as the one at TIQI, H_2^+ ions are co-trapped with beryllium ions ($^9Be^+$). The $^9Be^+$ ions are instrumental in sympathetically cooling the H_2^+ molecules, effectively reducing their kinetic energy and minimizing Doppler broadening of spectral lines. This cooling process is crucial as it provides a colder and more controlled environment, thereby enhancing the precision of spectroscopic measurements.

Additionally, the use of $^9Be^+$ ions facilitates the implementation of quantum logic spectroscopy (QLS). In QLS, an auxiliary ion such as $^9Be^+$ takes over the tasks of laser cooling and state detection. This technique transfers the quantum state information from the target ion H_2^+ to the auxiliary ion, making it easier to detect and manipulate with high precision. QLS thus enables us to probe H_2^+ with exceptional accuracy by leveraging the well-understood properties of the auxiliary ion.

Furthermore,$^9Be^+$ ions enable the characterization of the magnetic field environment within the trap, as explained in [14]. Accurate knowledge of the magnetic field is essential for ensuring that the magnetic field insensitive transitions in H_2^+ are correctly measured. This characterization relies on understanding the hyperfine interactions and energy levels of $^9Be^+$. By analyzing the hyperfine structure, we can monitor and control the magnetic field more effectively, which is critical for maintaining the stability of the experimental setup and for accurate spectroscopic studies.

We will proceed similarly as we have done for H_2^+, to differentiate the quantities concerning the $^9Be^+$ ion from the ones of the H_2^+ molecule, we will note these with a tilde on the top. First we look at the coupling scheme, then at the effective spin Hamiltonian $\tilde{H}_{eff}$ and finally we obtain the hyperfine states.

3.1 The angular momentum coupling scheme

For the $^9Be^+$ ion, the energy states are defined by the nuclear spin $\tilde{\mathbf{I}}$ and the electronic angular momentum $\tilde{\mathbf{J}} = \tilde{\mathbf{S}}_\mathbf{e} + \tilde{\mathbf{L}}$. Again we couple these two angular momenta to obtain the total coupled angular momentum $\tilde{\mathbf{F}} = \tilde{\mathbf{J}} + \tilde{\mathbf{I}}$, so we have the vector-space $\tilde{V}_F = \tilde{V}_J \bigotimes \tilde{V}_I$. The coupled basis for the hyperfine structure is $|((\tilde{S}_e, \tilde{L})\tilde{J}, \tilde{I})\tilde{F}, \tilde{m}_F\rangle$.

The nuclear spin of $^9Be^+$ is $\tilde{I} = \frac{3}{2}$. Here, we examine the three lowest states of this ion, which can be labeled either using spectroscopic notation or as $(\tilde{L}, \tilde{J})$. The ground state is $^2S_{1/2}$, where $\tilde{L} = 0$ and the only possible value for the total angular momentum is $\tilde{J} = \frac{1}{2}$. Next, for $\tilde{L} = 1$, we have two possible electronic angular momenta, $\tilde{J} = 1 \pm \frac{1}{2}$, corresponding to the excited states $^2P_{1/2}$ and $^2P_{3/2}$ respectively.

3.2 The effective spin Hamiltonian

As before we can write the effective spin Hamiltonian for each level, given by $(\tilde{L}, \tilde{J})$, as $\tilde{H}_{eff} = \tilde{H}_{hf} + \tilde{H}_Z$. We can express these operators as:

$$\tilde{H}_{hf} = A_{hf}(\tilde{\mathbf{I}} \cdot \tilde{\mathbf{J}}) + B_{hf}\mathbf{Q}(\tilde{\mathbf{I}}, \tilde{\mathbf{J}}), \tag{3.1}$$

$$\tilde{H}_Z = -(\tilde{\mu} \cdot \mathbf{B}), \tag{3.2}$$

In these equations we have introduced the coupling constants (A_{hf},B_{hf}), which have been measured experimentally for the levels we consider. The A_{hf} coefficient for $^2S_{1/2}$ is given in [16] and for the other levels they can be found in [15]. A big difference from the previous section is discussed in [16], here the coefficient A_{hf} has some magnetic field dependence. The formula used for the correction is $A_{hf}(B) = (1 + kB^2)A_{hf}$, where the diamagnetic shift coefficient is $k = 2.63 \times 10^{-11}T^{-2}$.

The other quantity that is introduced is the quadrupole term $\mathbf{Q}(\tilde{\mathbf{I}}, \tilde{\mathbf{J}})$, it only plays a role, when the electronic angular momentum is not minimal. Here only for the state $^2P_{3/2}$ (with $\tilde{J} = \frac{3}{2}$), for all other terms we have $B_{hf} = 0$. We can express the quadrupole term as:

$$\mathbf{Q}(\tilde{\mathbf{I}}, \tilde{\mathbf{J}}) = \frac{1}{2} \quad \frac{3(\tilde{\mathbf{I}} \cdot \tilde{\mathbf{J}})^2 + \frac{3}{2}(\tilde{\mathbf{I}} \cdot \tilde{\mathbf{J}}) - \tilde{\mathbf{I}}^2\tilde{\mathbf{J}}^2}{\tilde{I}(2\tilde{I} - 1) \times \tilde{J}(2\tilde{J} - 1)}, \tag{3.3}$$

The matrix elements of the Hamiltonian $\tilde{H}_{hf}$ are calculated in analogy from the ones in the previous section. To calculate the matrix elements of the Zeeman Hamiltonian, we still have to determine the magnetic dipole moment operator for this ion. We can again express this as the rank 1 tensor operator:

$$\tilde{\mu}^{(1)} = -g'_I \mu_B \tilde{\mathbf{I}}^{(1)} - g_J(\tilde{L}, \tilde{J}), \mu_B \tilde{\mathbf{J}}^{(1)}, \tag{3.4}$$

The g-factors g'_I and g_J have been measured in [16]. With this we can calculate the Hamiltonian matrix in the coupled basis $|\tilde{F}, \tilde{m}_F\rangle$ as we have done for H_2^+ in the previous chapter. In this case the matrix is less complicated and the resulting structure simpler. We have three different types of matrix elements in our effective spin Hamiltonian, we can write them as:

$$\langle \tilde{F}, \tilde{m}_F | \, (\tilde{\mathbf{I}} \cdot \tilde{\mathbf{J}}) \, | \tilde{F}', \tilde{m}'_F \rangle = \frac{1}{2}(\tilde{F}(\tilde{F}+1) - \tilde{I}(\tilde{I}+1) - \tilde{J}(\tilde{J}+1))\delta_{\tilde{F}\tilde{F}'}\delta_{\tilde{m}_F\tilde{m}'_F}, \tag{3.5}$$

$$\begin{aligned} \langle \tilde{F}, \tilde{m}_F | \, (\tilde{\mathbf{I}})^{(1)}_q \, | \tilde{F}', \tilde{m}'_F \rangle = C^{\tilde{F},\tilde{m}_F}_{\tilde{F}',\tilde{m}'_F;1,q}(-1)^{\tilde{F}+\tilde{J}+\tilde{I}'+1} \begin{Bmatrix} \tilde{I} & 1 & \tilde{I}' \\ \tilde{F}' & \tilde{J} & \tilde{F} \end{Bmatrix} \\ \times \sqrt{2\tilde{F}'+1}\sqrt{\tilde{I}(\tilde{I}+1)(2\tilde{I}+1)}\delta_{\tilde{J}\tilde{J}'}, \end{aligned} \tag{3.6}$$

$$\begin{aligned} \langle \tilde{F}, \tilde{m}_F | \, (\tilde{\mathbf{J}})^{(1)}_q \, | \tilde{F}', \tilde{m}'_F \rangle = C^{\tilde{F},\tilde{m}_F}_{\tilde{F}',\tilde{m}'_F;1,q}(-1)^{\tilde{F}'+\tilde{J}+\tilde{I}+1} \begin{Bmatrix} \tilde{J} & 1 & \tilde{J}' \\ \tilde{F}' & \tilde{I} & \tilde{F} \end{Bmatrix} \\ \times \sqrt{2\tilde{F}'+1}\sqrt{\tilde{J}(\tilde{J}+1)(2\tilde{J}+1)}\delta_{\tilde{I}\tilde{I}'}. \end{aligned} \tag{3.7}$$

By adding and multiplying matrices involving these operators, we can recover an expression for the full Hamiltonian matrix H_{eff}.

3.3 Eigenstates

For each level $(\tilde{L}, \tilde{J})$ we have the states $|\tilde{F}, \tilde{m}_F\rangle$, where $\tilde{F}$ ranges from $(\tilde{J} + \tilde{I})$ to $|\tilde{J} - \tilde{I}|$. We have chosen to order the states first increasing in $\tilde{F}$ and then in $\tilde{m}_F$. At the zero field, these are the exact eigenstates of the Hamiltonian, with a degeneracy in the angular momentum projection $\tilde{m}_F$. The energies of all the levels considered at zero field are displayed in table 3.1.

With a magnetic field, this degeneracy is lifted, and as the magnetic field increases, the states get more mixed, because the Zeeman Hamiltonian has non-vanishing off-diagonal terms. The hyperfine states for the three levels considered are plotted in 3.1 for a range of magnetic field values B.

Ground Electronic State of ^{9}Be$^+$ Nuclear spin $\tilde{I} = \frac{3}{2}$	
State $\|\tilde{F}\rangle$	**Energy (MHz)**
Level $^2S_{1/2}$	
$\|1\rangle$	781.26104631
$\|2\rangle$	-468.75662778
Level $^2P_{1/2}$	
$\|1\rangle$	147.415
$\|2\rangle$	-88.449
Level $^2P_{3/2}$	
$\|0\rangle$	0.97325
$\|1\rangle$	2.24665
$\|2\rangle$	2.49405
$\|3\rangle$	-2.88335

Table 3.1: Hyperfine energy levels for the lowest electronic states of ^{9}Be$^+$.

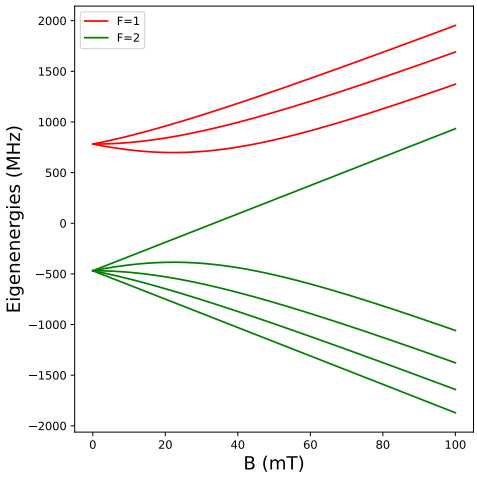

(a) Level $^2S_{1/2}$

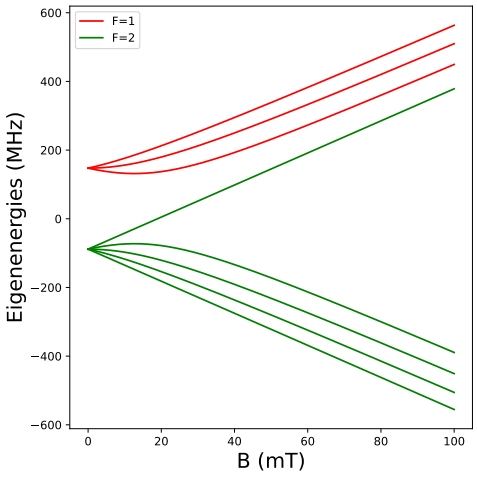

(b) Level $^2P_{1/2}$

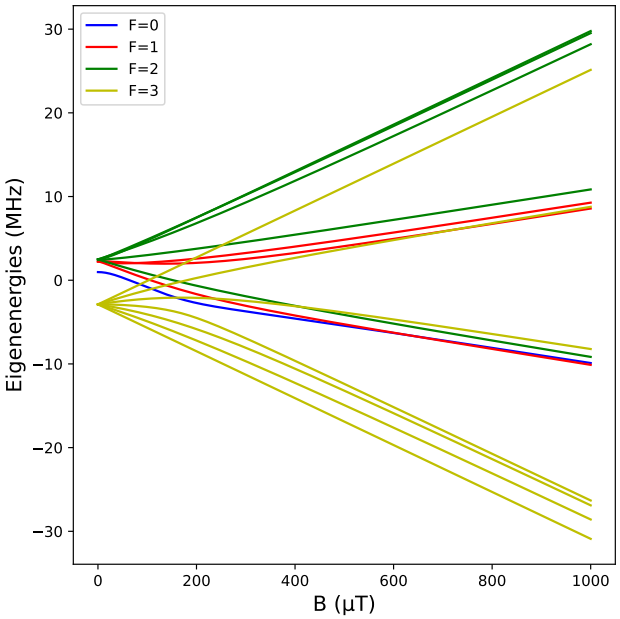

(c) Level $^2P_{3/2}$

Figure 3.1: Hyperfine states plotted against magnetic field values for the different levels in $^9Be^+$. For the last level with the richest structure in subplot 3.1(c), a smaller magnetic field range is chosen, as the hyperfine splitting for this level is of orders of magnitude smaller than the other two, as shown in table 3.1.

Chapter 4

Hyperfine transitions

In this chapter, we will look at different transitions in the hyperfine manifold of one ro-vibrational level (ν, L) of H_2^+ and between hyperfine states of two different ro-vibrational levels. First we will search for magnetic field strengths at which transitions are insensitive, meaning that the energy difference between the two states considered (and also the transition frequency) barely changes when the magnetic field B varies about that value. Next, we will look at the actual transition mechanisms that are achievable. For the insensitive transitions found before, we will compute the transition probabilities to determine if the transitions are allowed.

4.1 Magnetic field insensitive transitions

Considering magnetic field insensitive transitions is crucial for several reasons related to precision measurements, reducing experimental uncertainties, and obtaining clearer spectral lines. Laboratory environments often have fluctuating magnetic fields, which can introduce noise and variability in spectroscopic measurements. These magnetic field variations can cause unwanted shifts and broadenings in sensitive transitions, complicating data analysis and reducing the precision of measurements. By focusing on magnetic field insensitive transitions, the impact of these environmental fluctuations is minimized, resulting in more stable and repeatable measurements.

When talking about insensitive transitions, we consider the transition insensitive if the sensitivity s, is below a certain threshold. The range of values in which the transition is considered insensitive is noted as (B_{min}, B_{max}) and the value at which the sensitivity is minimal in this interval is denoted as B_s. The range of magnetic field values is probed with accuracy of 10 nT ($= 10^{-5}$ mT) for this purpose in the

1 mT range. These values are arbitrary in principle, if in some case one of these values is chosen differently, it will be stated.

4.1.1 The ortho-groundstate

The ortho-groundstate $(0, 1)$ is split into 18 hyperfine states as shown in table 2.2 and schematically in figure 2.2 for a magnetic field of $B = 450$ μT. These states vary as the magnetic field varies. In figure 4.1 they are displayed in the magnetic field range of 1 mT. To find insensitive transitions, we have to find fields B at which two lines in the figure 4.1 are parallel. This corresponds to the points at which the derivatives of their energy with respect to the magnetic field $\frac{dE}{dB}$ are equal. For this reason the derivatives have been computed and are displayed in figure 4.2. The insensitive transitions correspond to crossing points of two lines in this figure as we can express the sensitivity between states $|i(B)\rangle$ and $|f(B)\rangle$ as:

$$s_{if} = \frac{dE_f}{dB} - \frac{dE_i}{dB}, \tag{4.1}$$

Here we consider the transition insensitive if the sensitivity is below the threshold $|s_{if}| \leq 10$ MHz/T. In fact for all the cases where this occurs, here the lines do actually cross. As seen in the figure 4.2, there are multiple such crossing points in this range.

For a better overview of these insensitive transitions, they are all put into the table 4.1. In this table the range considered is extended up to 1.2 mT. The reason for that is that as one can see in the figure 4.2, the lines of state $|3\rangle$ and state $|15\rangle$, which cross at $B_s = 277.94$ μT, seem to collide again at the end. And after computation, as done in table 4.1, we see that this transition is in fact insensitive again at $B_s = 1008.29$ μT and thus is insensitive twice in this range.

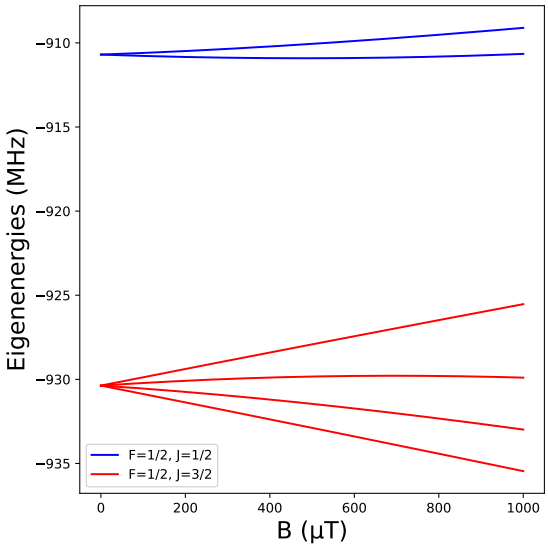

(a)

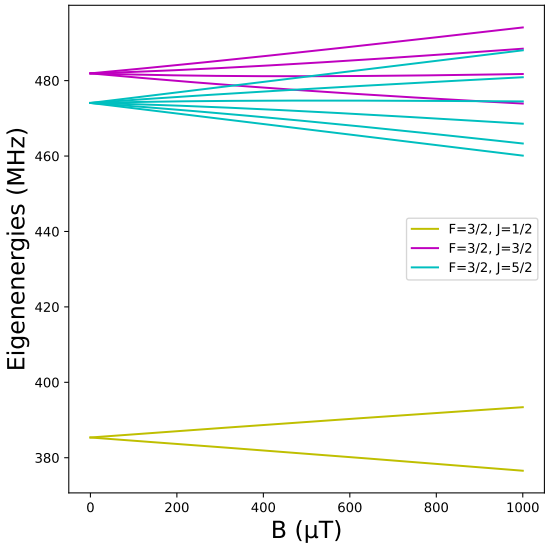

(b)

Figure 4.1: The two subplots show the hyperfine states of the Ortho-groundstate in the 1 mT range. They are splitted into two figures as the energy difference between states with different total spins F is large. In 4.1(a) we have the $F = \frac{1}{2}$ and in 4.1(b) the $F = \frac{3}{2}$ sub-levels. We can see that for some levels, the behaviour is not entirely linear in this range.

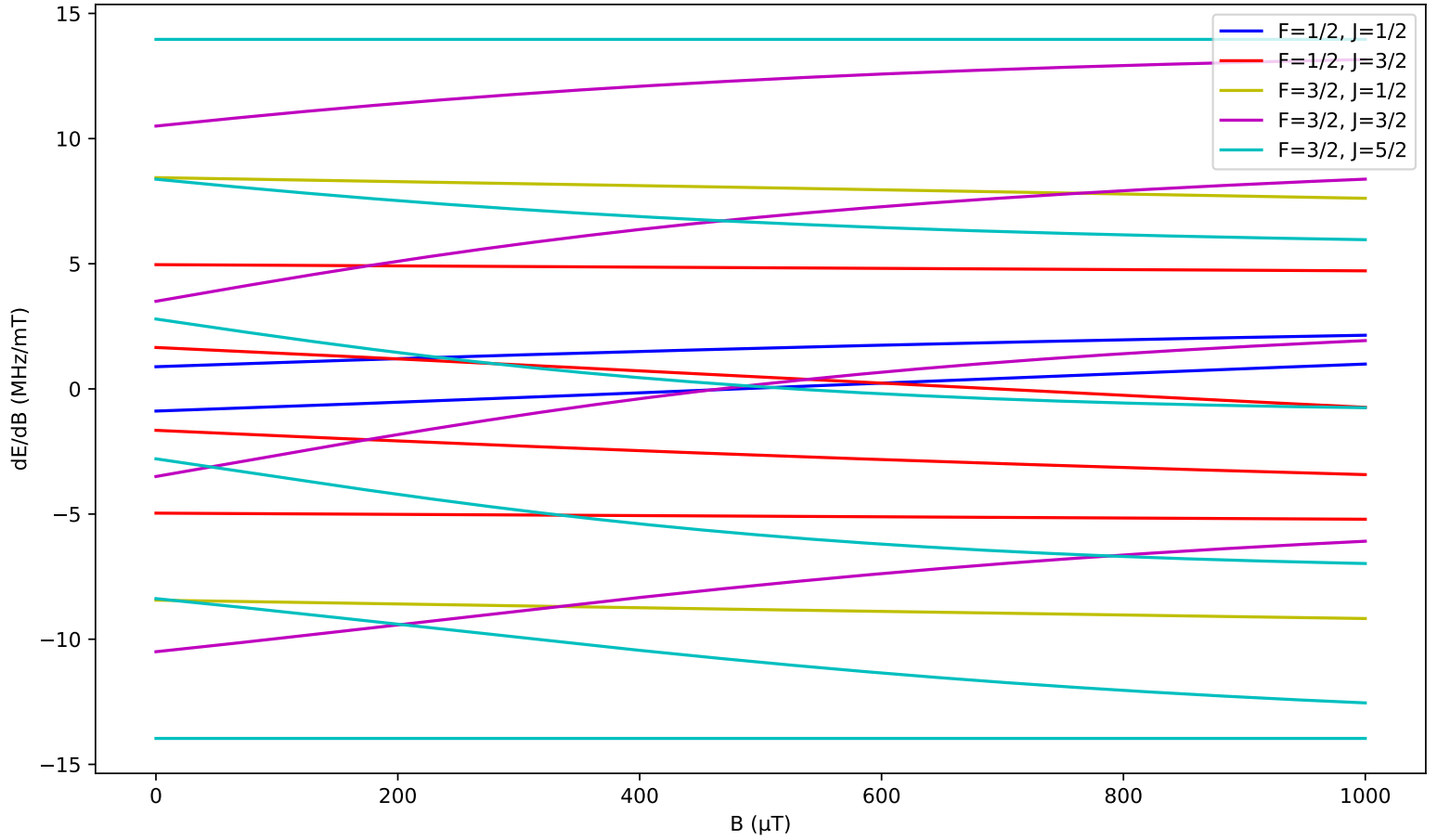

Figure 4.2: The derivatives of the hyperfine energies of the ortho-groundstate with respect to the magnetic field $\frac{dE}{dB}$ in the 1 mT range. As many of these lines are not constant, we can see many crossing points. The two lines with the highest and lowest values correspond to the stretched states of this level. We can clearly see, that these lines are completely straight, as the states are pure.

Initial State				Final State				Frequency	Insensitivity Range [μT]		
i	$(F,$	$J,$	$M_J)$	f	$(F,$	$J,$	$M_J)$	f_{hf} [MHz]	$(B_{\min},$	$B_{\max})$	B_{s}
6	$\frac{3}{2}$	$\frac{1}{2}$	$-\frac{1}{2}$	13	$\frac{3}{2}$	$\frac{5}{2}$	$-\frac{3}{2}$	88.7101	12.84	17.73	15.29
9	$\frac{3}{2}$	$\frac{3}{2}$	$-\frac{1}{2}$	14	$\frac{3}{2}$	$\frac{5}{2}$	$-\frac{1}{2}$	7.8314	44.30	45.56	44.93
4	$\frac{1}{2}$	$\frac{3}{2}$	$+\frac{1}{2}$	9	$\frac{3}{2}$	$\frac{3}{2}$	$-\frac{1}{2}$	1412.1348	173.71	175.66	174.69
2	$\frac{1}{2}$	$\frac{3}{2}$	$-\frac{3}{2}$	10	$\frac{3}{2}$	$\frac{3}{2}$	$+\frac{1}{2}$	1412.1686	174.56	177.13	175.84
1	$\frac{1}{2}$	$\frac{1}{2}$	$+\frac{1}{2}$	3	$\frac{1}{2}$	$\frac{3}{2}$	$-\frac{1}{2}$	19.5997	195.16	200.32	197.74
8	$\frac{3}{2}$	$\frac{3}{2}$	$-\frac{3}{2}$	13	$\frac{3}{2}$	$\frac{5}{2}$	$-\frac{3}{2}$	7.6292	201.26	203.09	202.17
1	$\frac{1}{2}$	$\frac{1}{2}$	$+\frac{1}{2}$	15	$\frac{3}{2}$	$\frac{5}{2}$	$+\frac{1}{2}$	1384.9864	231.99	234.77	233.38
3	$\frac{1}{2}$	$\frac{3}{2}$	$-\frac{1}{2}$	15	$\frac{3}{2}$	$\frac{5}{2}$	$+\frac{1}{1}$	1404.5916	274.48	281.45	277.94
6	$\frac{3}{2}$	$\frac{1}{2}$	$-\frac{1}{2}$	8	$\frac{3}{2}$	$\frac{3}{2}$	$-\frac{3}{2}$	96.2111	330.87	334.09	332.48
5	$\frac{1}{2}$	$\frac{3}{2}$	$+\frac{3}{2}$	14	$\frac{3}{2}$	$\frac{5}{2}$	$-\frac{1}{2}$	1404.7952	332.80	336.52	334.66
0	$\frac{1}{2}$	$\frac{1}{2}$	$-\frac{1}{2}$	9	$\frac{3}{2}$	$\frac{3}{2}$	$-\frac{1}{2}$	1392.0777	455.60	460.94	458.26
10	$\frac{3}{2}$	$\frac{3}{2}$	$+\frac{1}{2}$	16	$\frac{3}{2}$	$\frac{5}{2}$	$+\frac{3}{2}$	6.8241	466.66	469.46	468.05
9	$\frac{3}{2}$	$\frac{3}{2}$	$-\frac{1}{2}$	15	$\frac{3}{2}$	$\frac{5}{2}$	$+\frac{1}{2}$	6.4608	487.40	489.70	488.55
0	$\frac{1}{2}$	$\frac{1}{2}$	$-\frac{1}{2}$	15	$\frac{3}{2}$	$\frac{5}{2}$	$+\frac{1}{2}$	1385.6197	507.76	511.70	509.73
3	$\frac{1}{2}$	$\frac{3}{2}$	$-\frac{1}{2}$	9	$\frac{3}{2}$	$\frac{3}{2}$	$-\frac{1}{2}$	1410.9949	537.59	540.28	538.93
0	$\frac{1}{2}$	$\frac{1}{2}$	$-\frac{1}{2}$	3	$\frac{1}{2}$	$\frac{3}{2}$	$-\frac{1}{2}$	18.8975	598.17	602.70	600.44
7	$\frac{3}{2}$	$\frac{1}{2}$	$+\frac{1}{2}$	10	$\frac{3}{2}$	$\frac{3}{2}$	$+\frac{1}{2}$	94.9703	761.15	766.54	763.84
8	$\frac{3}{2}$	$\frac{3}{2}$	$-\frac{3}{2}$	14	$\frac{3}{2}$	$\frac{5}{2}$	$-\frac{1}{2}$	5.2398	786.04	789.89	787.96
3	$\frac{1}{2}$	$\frac{3}{2}$	$-\frac{1}{2}$	15	$\frac{3}{2}$	$\frac{5}{2}$	$+\frac{1}{2}$	1404.3865	1002.59	1013.94	1008.29
1	$\frac{1}{2}$	$\frac{1}{2}$	$+\frac{1}{2}$	9	$\frac{3}{2}$	$\frac{3}{2}$	$-\frac{1}{2}$	1390.8480	1172.97	1193.04	1182.93

Table 4.1: Possible magnetic field insensitive transitions of the ortho-ground state $(\nu, L) = (0, 1)$. The magnetic field range considered goes up to 1.2 mT. The sensitivity threshold is set to 10 MHz/T. The transitions that are dipole allowed have $|\Delta M_J| \leq 1$.

4.2 Magnetic dipole transitions (M1)

Magnetic dipole transitions (M1) are given by the magnetic dipole operator $\mu_q^{(1)}$ given by equation 2.14. Since this operator only couples states within the same rotational level L, these transitions obey the selection rule $\Delta L = 0$ in all cases. Here we only consider transitions within the same ro-vibrational level (ν, L), having $\Delta\nu = 0$. In [18], the more general case of such transitions has been considered. By computing the matrix element between the two hyperfine states involved in the transition, we obtain a quantity that is related to the transition probability by Fermis Golden Rule:

$$\left| \langle f | \frac{\mu_q}{\mu_B} | i \rangle \right|, \tag{4.2}$$

The reason we divide by Bohrs magneton μ_B is to obtain unitless numbers of order unity. These matrix elements are only nonzero if the projection of the total angular momentum of the two states obeys the equation:

$$M'_J - M_J = q, \tag{4.3}$$

This means that the magnetic dipole transition is possible for transitions with $|\Delta M_J| \leq 1$ and only for one choice of polarization given by equation 4.3. For all other transitions ($|\Delta M_J| \geq 2$), the magnetic dipole transitions are not possible.

The matrix elements for insensitive transitions in the 1 mT range for the ground vibrational level $\nu = 0$ and $L = 1, 2, 3$ are displayed in tables in the appendix C.1.

4.3 Two-photon transitions (2E1)

Electric dipole transitions (E1) are given by the electric dipole operator $\mathbf{d}$, defined by:

$$\mathbf{d} = e[(\mathbf{R_1} + \mathbf{R_2}) - \mathbf{R_e}], \tag{4.4}$$

where $\mathbf{R_1}$, $\mathbf{R_2}$, and $\mathbf{R_e}$ are the position vectors of the nuclei and of the electron with respect to the center of mass.

Electric dipole transitions change the orbital angular momentum as $|\Delta L| = 1$, but they also maintain the nuclear spin I (meaning $\Delta I = 0$). For that reason these transitions are called forbidden, as they are not allowed within the same band Σ_g

(or Σ_u). These dipole transitions between the different bands are allowed, but are very weak and will not be considered here.

Here we will consider two photon transitions as was done in [6]. They can be seen as two consecutive electric dipole transitions, where the intermediate state is only a virtual state. For that reason they are denominated as (2E1). The selection rules for these transitions are $\Delta L \in \{0, \pm 2\}$ and $\Delta I = 0$, which are allowed transitions for the bound Σ_g band states.

The operator that is considered for such transitions is the two-photon transition operator ${}^{S}Q_{\epsilon_1,\epsilon_2}(E) = \frac{1}{2}(Q_{\epsilon_1,\epsilon_2}(E) + Q_{\epsilon_2,\epsilon_1}(E))$, where E is the intermediate state energy and ϵ_i are the polarization vectors of the two photons. For spacing reasons often the energy as an argument is dropped in this case. The operator is expressed as:

$$Q_{\epsilon_1,\epsilon_2}(E) = \mathbf{d} \cdot \epsilon_{\mathbf{1}} \frac{1}{H - E} \mathbf{d} \cdot \epsilon_{\mathbf{2}}, \tag{4.5}$$

Here $\mathbf{d}$ is the dipole operator and H is the full Hamiltonian. The two-photon transition operator can also be written in cyclic coordinates, if the polarization vectors of the photons are chosen among the standard polarizations $(\pi, \sigma_+, \sigma_-)$. In this case the equations become:

$${}^{S}Q_{q_1,q_2} = \frac{1}{2}(Q_{q_1,q_2} + Q_{q_2,q_1}), \qquad\qquad Q_{q_1,q_2} = d_{q_1} \frac{1}{H - E} d_{q_2}, \tag{4.6}$$

To calculate the quantities $\left| \langle f(B)|^{S} Q_{q_1,q_2} |i(B)\rangle \right|^2$ that are related to the transition probability, the operator Q_{q_1,q_2} is written as a sum of irreducible tensor operators of rank 0 and 2:

$$Q_{q_1,q_2} = \sum_{k=0,2} \left(\sum_{q=-k}^{k} C^{k,q}_{1,q_1;1,q_2} \quad Q^{(k)}_q \right), \tag{4.7}$$

We can write the matrix elements as:

$$\begin{aligned} \langle f|^{S} Q_{q_1,q_2} |i\rangle &= \frac{1}{2} \langle f| \left(Q_{q_1,q_2} + Q_{q_2,q_1}\right) |i\rangle , \\ \langle f| Q_{q_1,q_2} |i\rangle &= C^{0,0}_{1,q_1;1,q2} \langle f| Q^{(0)}_0 |i\rangle + \sum_{q=-2}^{2} C^{2,q}_{1,q_1;1,q2} \langle f| Q^{(2)}_q |i\rangle , \end{aligned} \tag{4.8}$$

The tensor operators $Q_q^{(k)}$ only act on the orbital angular momentum subspace V_L, thus we can use the equation A.13 to calculate the matrix elements. For the pure states we find:

$$\langle \nu', L', F', J', M_J' |\, Q_q^{(k)} \,| \nu, L, F, J, M_J \rangle = C_{J,M_J;k,q}^{J',M_J'} (-1)^{J+L'+F+k} \sqrt{(2J+1)} \times \begin{Bmatrix} L' & k & L \\ J & F & J' \end{Bmatrix} \langle \nu', L' || \mathbf{Q}^{(k)} || \nu, L \rangle \, \delta_{FF'}, \tag{4.9}$$

The reduced matrix elements $\langle \nu', L' || \mathbf{Q}^{(k)} || \nu, L \rangle$ have been calculated numerically for different ro-vibrational levels in different papers. In [23] the reduced matrix elements for the para-groundstate $(\nu, L) = (0, 0)$ and the excited vibrational levels $\nu' = 1, 2, 3$ $(L' = 0)$ are calculated. This is a demonstration that the strength of this type of transitions decreases very strongly as the difference between vibrational levels increases. Thus, only the transitions with $\Delta\nu = 1$ are considered for two-photon transitions, this becomes kind of a selection rule. The reduced matrix elements for different transitions of this kind are calculated in [7] and in [17].

In Appendix C.2, the different feasible magnetic field insensitive two-photon transitions in the 1 mT range between the ortho-groundstate $(\nu, L) = (0, 1)$ and the first excited vibrational level $(\nu', L') = (1, 1)$ (with $\Delta\nu = 1$) are displayed.

4.4 Electric quadrupole transitions (E2)

Electric quadrupole transitions (E2) are allowed between states of the same band Σ_g (or Σ_u), since they are even with respect to parity and to permutation of the two protons. As the dipole transitions (E1) are not, these transitions are the dominant mode of decay of the hydrogen molecular ion. Electric quadrupole transitions have been considered in [17] and [19].

The quadrupole transition operator is of rank 2, its components can be written in Cartesian coordinates as $\{\Theta_{ij}\}_{i,j=1}^{3}$ as done in [17], resulting in a traceless symmetric matrix operator. To calculate the matrix elements proportional to the transition probability we express this tensor in cyclic coordinates $\{\Theta_q^{(2)}\}_{q=-2}^{2}$ with:

$$\Theta_{ij} = \sum_{q=-2}^{2} \Theta_q^{(2)} c_{ij}^{(q)}, \tag{4.10}$$

where the second rank tensors $c_{ij}^{(q)}$ are introduced, they are given explicitly in [20]. For photons of polarization $\vec{\epsilon}$ along the propagation direction $\vec{n}$, the matrix element that is to be considered for a transition between states $|i\rangle$ and $|f\rangle$ is:

$$\Theta_{\epsilon,n}^{if} = \frac{1}{3}\sum_{i,j=1}^{3}\sum_{q=-2}^{2} \langle f|\, \Theta_q^{(2)}\, |i\rangle\, c_{ij}^{(q)} \epsilon_i n_j, \tag{4.11}$$

To maximize the amplitude of the transition, the propagation direction and the polarization must be chosen in a certain way depending on the $|\Delta M|$ of the transition. This is because one has to maximize the geometrical factor $|g_q| = |\sum_{i,j} c_{ij}^{(q)} \epsilon_i n_j|$.

In the case $\Delta M_J = 0$ we find the maximal $|g_0| = \frac{1}{2}$ for $\vec{n}_0$ making an angle of $\frac{\pi}{4}$ with the quantization axis, and polarization $\vec{\epsilon}_0$ in the plane defined by $\vec{n}_0$ and the quantization axis $\vec{e_z}$. For $\Delta M_J = \pm 1$ we obtain a maximal $|g_{\pm 1}| = \frac{1}{\sqrt{6}}$ for propagation direction $\vec{n}_{\pm 1}$ orthogonal to the quantization axis $\vec{e_z}$ and polarization $\vec{\epsilon}_{\pm 1}$ along $\vec{e_z}$. In the case $\Delta M_J = \pm 2$ propagation direction $\vec{n}_{\pm 2}$ orthogonal to the z axis, and polarization $\vec{\epsilon}_{\pm 2}$ orthogonal to the plane defined by $\vec{n}_{\pm 2}$ and the axis $\vec{e_z}$ lead to a maximal $|g_{\pm 2}| = \frac{1}{\sqrt{6}}$.

We can write the matrix element $\langle f|\, \Theta_q^{(2)}\, |i\rangle$ in terms of a reduced matrix element, the same way as for the tensor operators of two-photon transitions in 4.9, resulting in the equation:

$$\begin{aligned}\langle \nu', L', F', J', M_J'|\, \Theta_q^{(2)}\, |\nu, L, F, J, M_J\rangle = C_{J,M_J;2,q}^{J',M_J'}(-1)^{J+L'+F}\sqrt{(2J+1)} \\ \times \begin{Bmatrix} L' & 2 & L \\ J & F & J' \end{Bmatrix} \langle \nu', L'||\mathbf{\Theta}^{(2)}||\nu, L\rangle\, \delta_{FF'},\end{aligned} \tag{4.12}$$

These reduced matrix elements $\langle \nu', L'||\mathbf{\Theta}^{(2)}||\nu, L\rangle$ have been calculated in the supplementary material of [21] between all states with $0 \leq \nu \leq 10$ and $0 \leq L \leq 6$. We find that, in contrast to the (2E1) transitions, these (E2) transition matrix elements do not drop off as fast with increasing $\Delta\nu$. In any case, they are smaller for this kind of transitions. The transition rates then scale with the intensity of the light. For quadrupole transitions, the rates scale linearly with intensity, and for two-photon transitions, the rates scale quadratically with intensity.

In Appendix C.3, we display different feasible magnetic field insensitive quadrupole transitions between the groundstate and excited levels for both ortho- and para-H_2^+.

Chapter 5

Systematic frequency shifts

When we trap H_2^+ in an experimental setup, the energy levels and transition frequencies that are observed may differ from the ones calculated in the previous section because of the environment. On the one hand, in an ion trap we have static electrical fields that lead to a quadrupole shift on the hydrogen molecular ions. On the other hand, if we drive transitions using lasers, these lead to light shifts between the energy levels that are driven.

In this section, these shifts are treated with the goal to be able to predict the frequencies with higher accuracy.

5.1 Quadrupole shift

The electric quadrupole shift has been treated extensively in [22] in the Born–Oppenheimer approximation. They concluded that the effects of the quadrupole interaction can be treated in the form of an additional term V_Q in the effective spin Hamiltonian H_{eff}.

$$V_Q(\nu, L) = \sqrt{\frac{3}{2}} E_{14}(\nu, L) Q(\mathbf{R_C})(\mathbf{L} \otimes \mathbf{L})^{(2)}, \tag{5.1}$$

Here the E_{14} are numerical coefficients, that have to be calculated for each rovibrational level (ν, L). They were calculated for $0 \leq \nu \leq 8$ and $0 \leq L \leq 10$ in [22]. The second term is the gradient of the static external electric field at the center of mass coordinate $\mathbf{R_C}$, in Cartesian coordinates $Q_{ij} = \partial_i E_j$. To be exact one has to write this operator in cyclic components the other way around as done for the quadrupole operator, finding an equation equivalent to 4.10 but inverted:

$$\hat{Q}_q^{(2)} = \frac{3}{2}\sum_{ij} Q_{ij}(-1)^q c_{ij}^{(-q)}, \tag{5.2}$$

where the relations for the $c_{ij}^{(q)}$ stated in [20] are used to invert the equation. This operator is not to be confused with the one appearing for the two-photon transitions, for that reason the hat notation is introduced. The product appearing in equation 5.1 can be expressed as:

$$\begin{aligned} Q(\mathbf{R_C})(\mathbf{L}\otimes\mathbf{L})^{(2)} &= \sum_{q=-2}^{2}(-1)^q \hat{Q}_{-q}^{(2)}(\mathbf{L}\otimes\mathbf{L})_q^{(2)}, \\ &= \sum_{q=-2}^{2}\sum_{i,j}\frac{3}{2}Q_{ij}c_{ij}^{(q)}(\mathbf{L}\otimes\mathbf{L})_q^{(2)}, \end{aligned} \tag{5.3}$$

If the trapping potential is complicated, we could have up to 5 nonzero such components. Instead if the trapping potential only varies along the quantization axis, the only component that we have is the one for $q = 0$ and the expression for the quadrupole term becomes:

$$V_Q(\nu, L) = \sqrt{\frac{3}{2}}E_{14}(\nu, L)Q_{zz}(\mathbf{L}\otimes\mathbf{L})_0^{(2)}, \tag{5.4}$$

Back to the general case. The quadrupole interaction V_Q is a rank 0 tensor operator, it is diagonal in (J, M_J) by the Wigner-Eckart theorem A.9. Since the equation becomes very long, here we split it in three steps. Where the second and third equations give explicit expressions for reduced matrix elements that can be found in the equation above.

$$\langle F', J, M_J|\, V_Q\, |F, J, M_J\rangle = \left(\frac{3}{2}\right)^{\frac{3}{2}} E_{14}(\nu, L)\sum_{ij} Q_{ij}c_{ij}^{(q)}\, \langle F', J, M_J|\, (\mathbf{L}\otimes\mathbf{L})_q^{(2)}\, |F, J, M_J\rangle\,, \tag{5.5}$$

$$\begin{aligned} \langle F', J|\,|(\mathbf{L}\otimes\mathbf{L})^{(2)}|\,|F, J\rangle &= (-1)^{J+L'+F}\sqrt{(2J+1)} \\ &\times \begin{Bmatrix} L' & 2 & L \\ J & F & J \end{Bmatrix} \langle L||(\mathbf{L}\otimes\mathbf{L})^{(2)}||L\rangle\, \delta_{FF'}, \end{aligned} \tag{5.6}$$

$$\langle L||(\mathbf{L}\otimes\mathbf{L})^{(2)}||L\rangle = \sqrt{\frac{L(L+1)(2L-1)(2L+1)(2L+3)}{6}}, \tag{5.7}$$

Where the reduced matrix element in equation 5.7 has been calculated by decomposing the tensor operator into the rank 1 known tensor operators $\mathbf{L}^{(1)}$:

$$(\mathbf{L}\otimes\mathbf{L})^{(2)}_q = \sum_{q'=-1}^{1} C^{2,q}_{1,q';1,(q-q')} L^{(1)}_{q'} L^{(1)}_{q-q'}, \tag{5.8}$$

With equation 5.6 (together with the WE-theorem) we see that this Hamiltonian is diagonal in the $|F, J, M_J\rangle$ basis. One way to incorporate this interaction would be to treat it perturbatively and add the resulting shift to the hyperfine energy of each state. Instead of doing that, we can treat it exactly by adding it to the effective spin Hamiltonian as mentioned in the beginning, finding:

$$H_{eff} = H_{hf} + H_Z + V_Q, \tag{5.9}$$

Diagonalizing this Hamiltonian we obtain a new hyperfine basis, taking into account the quadrupole interaction.

5.2 Static polarizability and the DC Stark shift

While the ion in an ideal trap is located at the field null, practical setups often exhibit imperfections, such as stray electric fields or slight misalignments, which result in a small but non-zero electric field at the ion's position. This residual field can induce a DC Stark shift in the hyperfine states of H_2^+. Even though this shift may be small, it is important to consider and quantify it for high-precision spectroscopy.

When interacting with an external electric field $\mathbf{E}$ in the dipole interaction, the change of energy due to the polarizability of a molecular ion is expressed by

$$E_p^{(2)} = E_i E_j \langle\psi_0| d_i \frac{1}{H_0 - E_0} d_j |\psi_0\rangle = -\frac{1}{2}\alpha_d^{ij} E_i E_j, \tag{5.10}$$

where $|\psi_0\rangle$ are the eigenstates of energy E_0 of the non-relativistic Hamiltonian H_0 and α_d^{ij} , the polarizability tensor of rank 2, has been introduced as in [24]. This tensor can be decomposed into irreducible tensors with a scalar term α_s and a tensor term α_t.

Now we introduce the polarizability operator $\hat{\alpha}_d$, to evaluate the polarizabilities of the hyperfine states of a given ro-vibrational level. The approximation that is made is that this operator only acts in a manifold of given L. We can write:

$$\hat{\alpha}_d^{ij}(\nu, L) = \alpha_s(\nu, L)\delta_{ij} + \alpha_t(\nu, L)[L_i L_j + L_j L_i - \frac{2}{3}\mathbf{L}^2\delta_{ij}], \tag{5.11}$$

The values of $\alpha_s(\nu, L)$ and $\alpha_t(\nu, L)$ were calculated in [24] and later in [25] relativistic corrections were included. Instead of using this decomposition into a scalar (rank 0) and a rank 2 irreducible tensor operator, it is more useful to write the polarizability along the quantization axis and orthogonal to it, making use of the cylindrical symmetry of the problem. This leads to the linear combinations:

$$\hat{\alpha}_\parallel(\nu, L) = \alpha_s(\nu, L) + \alpha_t(\nu, L)\sqrt{\frac{8}{3}}(\mathbf{L} \otimes \mathbf{L})_0^{(2)}, \tag{5.12}$$

$$\hat{\alpha}_\perp(\nu, L) = \alpha_s(\nu, L) - \frac{1}{2}\alpha_t(\nu, L)\sqrt{\frac{8}{3}}(\mathbf{L} \otimes \mathbf{L})_0^{(2)}, \tag{5.13}$$

Now we know how to calculate matrix elements involving the parallel and perpendicular polarizability for each hyperfine basis state $|F, J, M_J\rangle$ for all ro-vibrational levels (ν, L) and thus each eigenstate of the Hamiltonian H_{eff}. Another useful quantity to introduce is $\hat{\alpha}_\theta = \cos^2\theta\hat{\alpha}_\parallel + \sin^2\theta\hat{\alpha}_\perp$, the polarizability at a certain angle θ with respect to the quantization axis.

When the ion is in an external static electric field $\vec{E}$, the (DC) Stark energy shift induced to the eigenstate can be calculated using first order perturbation theory, if it is small compared to the other effects:

$$\Delta E_{DC}(i) = -\frac{1}{2}\left(\langle i|\,\hat{\alpha}_\parallel\,|i\rangle\, E_z^2 + \langle i|\,\hat{\alpha}_\perp\,|i\rangle\,(E_x^2 + E_y^2)\right), \tag{5.14}$$

When using this equation, one has to be careful to use the right units for the polarizabilities, as in the literature (in [24] and [25]) these are given in atomic units (au).

5.3 Light shifts

When driving a transition within the molecule with a laser, the energy levels can be shifted due to the (AC) Stark effect. This effect occurs due to the interaction

between the molecule and the dynamic electric field of the laser. These shifts have been theoretically studied in [17] for the two type of transitions between different ro-vibrational levels discussed before ((2E1) and (E2)).

When doing QLS like for the pair of $^9Be^+$ and H_2^+ we have Rabi oscillations with Rabi frequency Ω. The expression for this frequency will be different depending on the type of transition considered. In [20] a derivation is stated on how to obtain the Rabi requency for electric dipole (E1) and quadrupole (E2) transitions.

QLS clocks are typically operated with a single interrogation π-pulse whose duration τ is adjusted according to the desired resolution, typically of the order of 100 ms. The laser intensity I needed to obtain that duration is obtained by the relation $\Omega\tau = \pi$, as the Rabi frequency depends on the intensity. For simplicity, we will assume the use of this π-pulse method in our discussion, although other techniques such as Ramsey protocols are also viable options.

For photons of polarization ϵ and angular frequency ω, the dynamical polarizability of a state $|i\rangle$ is given by:

$$\alpha_\epsilon^i(\omega) = -4\pi a_0^3 \langle i| \left({}^S Q_{\epsilon\epsilon}(E_i + \hbar\omega) + {}^S Q_{\epsilon\epsilon}(E_i - \hbar\omega) \right) |i\rangle \,, \tag{5.15}$$

Where a_0 is the Bohr radius. These polarizabilities would have to be calculated numerically for each state and each transition wavelength. Here we will approximate them with the static polarizability ($\alpha_\epsilon^i(\omega) \approx \alpha_\epsilon^i(0)$). For most of the transitions this approximation is accurate enough, as for most of the states considered they only differ by at most a few percent.

The frequency the transition is shifted by is Δf_{LS}. This shift depends two things, one is the difference of the dynamic polarizability of the two states $\Delta\alpha_\epsilon^{if}$, which we will only be able to approximate using the difference of the static polarizabilities. The other is the intensity of the laser I or equivalently the amplitude of the electric field E_0, which are related by:

$$I = \frac{1}{2} c \epsilon_0 E_0^2, \tag{5.16}$$

Where c is the speed of light and ϵ_0 is the permittivity of the vacuum. For the considered transitions we will express the frequency shift for a π-pulse of duration τ, inserting the corresponding relationship between intensity I (or equivalently E_0) and Rabi frequency Ω.

5.3.1 Two-photon transitions (2E1)

We consider a transition between the state $|i\rangle$ and $|f\rangle$, each photon has frequency $\frac{E_f - E_i}{2}$, the factor half is important as we have to apply only half the correction on each photon to account for the shift. The Rabi frequency and the corresponding shift in the transition frequency (for each one of the two photons) needed to achieve a π-pulse of duration τ are given by:

$$\Omega = \frac{I}{\epsilon_0 \hbar c} \Big| \langle f |^S Q_{\epsilon\epsilon} | i \rangle \Big|, \tag{5.17}$$

$$\Delta f_{LS} = -\frac{1}{8\tau} \frac{\Delta \alpha_\theta^{if}}{| \langle f |^S Q_{\epsilon\epsilon} | i \rangle |}, \tag{5.18}$$

where for the shift in equation 5.18 both the polarizabilites and two-photon transition matrix elements are given in atomic units (au). The polarizability is given in units of $4\pi a_0^3$ and the matrix element in units of $\frac{\hbar^2 e^2}{m_e}$ in atomic units. The reason for this choice is that in the calculations these quantities are already expressed as such. If these quantities were expressed in SI units, we would have to change the equation.

Now we can calculate the shift in the transition frequency for any laser of polarization ϵ driving the two-photon transition between any two hyperfine states, for which we have calculated the transition matrix element. For example we can calculate the shift for the insensitive transitions found in table C.2 between the ortho-groundstate $(\nu_i, L_i) = (0, 1)$ and $(\nu_f, L_f) = (1, 1)$.

Note that in the table C.2 the total shift between the two levels is calculated for all of the frequencies. Since these are two-photon transitions, the shift that has to be applied to each one of the photons is only half of the values indicated in the table.

5.3.2 Electric quadrupole transitions (E2)

For quadrupole transitions we obtain equivalent expressions for both the Rabi frequency and the frequency shift:

$$\Omega = \frac{e a_0^2 E_0}{2\hbar} \frac{2\pi}{\lambda} \big| \Theta_{\epsilon n}^{if} \big|, \tag{5.19}$$

$$\Delta f_{LS} = -\frac{m_e \lambda^2}{4\hbar\tau^2} \frac{\Delta \alpha_\theta^{if}}{|\Theta_{\epsilon n}^{if}|^2}, \tag{5.20}$$

Again here the difference in polarizabilities and the transition matrix element are given in atomic units as for equation 5.18. For selected magnetic field insensitive transitions in the 1 mT range, the light shift of the transition frequency due to the AC-Stark shift has been calculated in the tables in the appendix C.

Ortho-transitions starting from the groundstate $(\nu_i, L_i) = (0, 1)$ to two different final states have been calculated, the final ro-vibrational state $(\nu_f, L_f) = (3, 1)$ and $(\nu_f, L_f) = (3, 3)$. One pair of para-H_2^+ is also considered in table C.5, where we have the initial para-groundstate $(\nu_i, L_i) = (0, 0)$ and the final state $(\nu_f, L_f) = (3, 2)$. For the transitions, that are drivable, meaning that the transition matrix element is big enough, the resulting shifts Δf_{LS} are small, of maximal a few kHz, compared to the hyperfine shifts introduced by our effective Hamiltonian Δf_{hf}, on the order of up to over 1 GHz. Nevertheless correcting for this shift is necessary for accurate measurements.

Appendix

Appendix A

Angular momentum structure

In this Appendix we derive the formalism for the angular momentum structure following [12], that is used in the previous chapters to treat the coupling of angular momenta and matrix elements.

When we have one angular momentum $\mathbf{J}$, it spans a $(2J+1)$ dimensional vectorspace V_J. The basis of this space that is considered, is that of simultaneous eigenstates of the operator $\mathbf{J}^2$ and the projection on the z-axis J_z (often called quantization axis and labeled J_0). Resulting in the $(2J+1)$ basis states $\{|J, M_J\rangle\}_{M_J \in \{-J,\dots,J\}}$ which posses the properties, that:

$$\begin{aligned} \mathbf{J}^2 |J, M_J\rangle &= J(J+1) |J, M_J\rangle , \\ J_z |J, M_J\rangle &= \quad M_J \quad |J, M_J\rangle , \end{aligned} \tag{A.1}$$

A.1 Coupling angular momenta

When dealing with two angular momenta $\mathbf{j_1}$ and $\mathbf{j_2}$, we have the tensorspace $V_1 \bigotimes V_2$ with the tensor basis $|j_1, m_1; j_2, m_2\rangle = |j_1, m_1\rangle \otimes |j_2, m_2\rangle$. By defining the coupled angular momentum operator:

$$\mathbf{J} = \mathbf{j_1} \otimes \mathbb{1} + \mathbb{1} \otimes \mathbf{j_2}, \tag{A.2}$$

Which is often written as $\mathbf{J} = \mathbf{j_1} + \mathbf{j_2}$, we have a new coupled angular momentum eigenbasis $|(j_1, j_2)J, M_J\rangle$ that can be expressed in terms of the uncoupled basis using the Clebsch-Gordan (CG) coefficients $C^{J,M_J}_{j_1,m_1;j_2,m_2} = \langle j_1, m_1; j_2, m_2 | J, M_J\rangle$ or equivalently the Wigner-3-j symbols.

$$
\begin{aligned}
|(j_1, j_2)J, M_J\rangle &= \sum_{m_1,m_2} C^{J,M_J}_{j_1,m_1;j_2,m_2} \, |j_1, m_1; j_2, m_2\rangle \\
&= \sum_{m_1,m_2} (-1)^{j_1-j_2+M_J} \sqrt{2J+1} \begin{pmatrix} j_1 & j_2 & J \\ m_1 & m_2 & -M_J \end{pmatrix} |j_1, m_1; j_2, m_2\rangle \,,
\end{aligned}
\tag{A.3}
$$

Often the letters in the brackets (j_1, j_2) are dropped, when it is clear what the coupled momentum J represents. In the case of only two angular momenta we actually have two choices for the coupling, depending on the chosen order of $\mathbf{j_1}$ and $\mathbf{j_2}$. They do not lead to the same basis. Not coupling as in A.3, changing the roles of $\mathbf{j_1}$ and $\mathbf{j_2}$, leads to a basis $|(j_2, j_1)J, M_J\rangle$ that differs for some states in the sign. The conversion factor is $(-1)^{j_1+j_2-J}$ for the two bases.

In the case that one wants to couple three angular momenta $\mathbf{j_1}$, $\mathbf{j_2}$ and $\mathbf{j_3}$, we have a new degree of freedom, as to the order in which the angular momenta are paired. One possible way to realize the coupling is by defining $\mathbf{J_{12}} = \mathbf{j_1} + \mathbf{j_2}$ (or $\mathbf{J_{23}} = \mathbf{j_2} + \mathbf{j_3}$) and then obtain the angular momentum operator $\mathbf{J} = \mathbf{J_{12}} + \mathbf{j_3}$ $(= \mathbf{j_1} + \mathbf{J_{23}})$. The different coupling schemes to reach $\mathbf{J}$ are all equally valid and would lead to different coupled angular momentum bases.

$$
|((j_1, j_2)J_{12}, j_3)J, M_J\rangle = \sum_{M_{12},m_3} C^{J,M_J}_{J_{12},M_{12};j_3,m_3} \sum_{m_1,m_2} C^{J_{12},M_{12}}_{j_1,m_1;j_2,m_2} \, |j_1, m_1; j_2, m_2; j_3, m_3\rangle \,,
\tag{A.4}
$$

$$
|(j_1, (j_2, j_3)J_{23})J, M_J\rangle = \sum_{m_1,M_{23}} C^{J,M_J}_{j_1,m_1;J_{23},M_{23}} \sum_{m_2,m_3} C^{J_{23},M_{23}}_{j_2,m_2;j_3,m_3} \, |j_1, m_1; j_2, m_2; j_3, m_3\rangle \,,
\tag{A.5}
$$

The Wigner-6-j symbols are defined to relate two bases for different coupling schemes, such that we can express one basis state of the first in terms of the states of the second basis:

$$
\begin{aligned}
|(J_{12}, j_3)J, M_J\rangle = (-1)^{j_1+j_2+j_3+J} &\sqrt{(2J_{12}+1)(2J_{23}+1)} \\
&\times \begin{Bmatrix} j_1 & j_2 & J_{12} \\ j_3 & J & J_{23} \end{Bmatrix} |(j_1, J_{23})J, M_J\rangle \,,
\end{aligned}
\tag{A.6}
$$

Using the equations A.4 and A.5 describing the coupled basis states in terms of the uncoupled basis, we can write the Wigner-6-j symbols in terms of CG-coefficients as:

$$\begin{Bmatrix} j_1 & j_2 & J_{12} \\ j_3 & J & J_{23} \end{Bmatrix} = \frac{(-1)^{j_1+j_2+j_3+J}}{\sqrt{(2J_{12}+1)(2J_{23}+1)}} \sum_{m_1,m_2,m_3,M_{12},M_{23}} C^{J,M_J}_{J_{12},M_{12};j_3,m_3} C^{J_{12},M_{12}}_{j_1,m_1;j_2,m_2} C^{J,M_J}_{j_1,m_1;J_{23},M_{23}} C^{J_{23},M_{23}}_{j_2,m_2;j_3,m_3}, \tag{A.7}$$

We can go further and couple 4 angular momenta and for that the 9-j symbols are defined. But for this analysis it suffices to know how to couple up to 3 angular momenta.

A.2 Irreducible tensor operators

In this section we will discuss the computation of matrix elements concerning tensor operators. A irreducible tensor operator $\mathbf{T}^{(k)}$ of rank k is a set of $2k+1$ operators $\{T^{(k)}_q\}^k_{q=-k}$ that transform into each other as angular-momentum states $\{|J,M\rangle\}^J_{M=-J}$. This means that they obey the equations:

$$\begin{aligned} [\mathbf{J}^2, T^{(k)}_q] &= k(k+1)T^{(k)}_q, \\ [J_z, T^{(k)}_q] &= qT^{(k)}_q, \end{aligned} \tag{A.8}$$

Where the square brackets $[\cdot,\cdot]$ denote the commutator of the two operators. This is in analogy to the angular momentum states in equations A.1, but instead of the action of a operator on a vector $|J,M\rangle$, we have the commutator of two operators, where the rank of the tensor $k = J$ and the component $q = M$. Any Cartesian tensor can be reduced into a sum of irreducible tensors.

A.3 Reduced matrix elements

When calculating matrix elements in this section, we will assume irreducible tensor operators, the result can be generalized by summation.

The basis considered is $|(\alpha)J, M_J\rangle$, where an additional parameter α is included, that represents other quantum numbers that do not represent angular dependence of the state. The matrix elements can thus in general be written as $\langle(\alpha)J, M_J|T_q^{(k)}|(\tilde{\alpha})\tilde{J}, \tilde{M}_J\rangle$.

An important result in angular momentum algebra is the Wigner-Eckart (WE) Theorem. It states, that matrix elements of such tensors can be written it as a product of a Wigner-3-j Symbol (or CG-coefficient) and a term that is independent of the projections of the angular momentum considered. The M_J and q independent term denoted $\langle(\alpha)J||T^{(k)}||(\alpha')J'\rangle$ is called the reduced matrix element.

$$\begin{aligned}\langle(\alpha)J, M_J|T_q^{(k)}|(\alpha')J', M'_J\rangle &= (-1)^{J-M_J}\begin{pmatrix} J & k & J' \\ -M_J & q & M'_J\end{pmatrix}\langle(\alpha)J||T^{(k)}||(\alpha')J'\rangle\,, \\ \langle(\alpha)J, M_J|T_q^{(k)}|(\alpha')J', M'_J\rangle &= \frac{1}{\sqrt{(2J+1)}}\quad C^{J,M_J}_{J',M'_J;k,q}\quad\langle(\alpha)J||T^{(k)}||(\alpha')J'\rangle\,,\end{aligned} \tag{A.9}$$

This equation differs from the equivalent in [12], where the convention has been used for the reduced matrix element with an extra factor of $\sqrt{2J+1}$. With that convention, the equation is simpler in the notation using the CG coefficients. The reason for the convention used here is that it is used in all the literature papers concerning the H_2^+ spectroscopy theory.

We can invert the equation using the symmetry relations of the Wigner-3-j symbols (equivalently the orthogonality relations of the CG-coefficients) to express the reduced matrix element as a sum over matrix elements.

$$\begin{aligned}\langle J||T^{(k)}||J'\rangle &= \sum_{M'_J,q}(-1)^{J-M_J}(2J+1)\begin{pmatrix} J & k & J' \\ -M_J & q & M'_J\end{pmatrix}\langle J, M_J|T_q^{(k)}|J', M'_J\rangle\,, \\ \langle J||T^{(k)}||J'\rangle &= \sum_{M'_J,q}\sqrt{(2J+1)}\quad C^{J,M_J}_{J',M'_J;k,q}\quad\langle J, M_J|T_q^{(k)}|J', M'_J\rangle\,,\end{aligned} \tag{A.10}$$

From this inverse Wigner-Eckart equation we can calculate two special cases for irreducible tensor operators of importance, the identity $\mathbb{1}$ and the angular momen-

tum operator $\mathbf{J}$, which are the rank 0 and 1 irreducible tensor operators. As for these operators the right hand side of equation A.10 can be simplified to obtain:

$$\langle J||\mathbb{1}||J'\rangle = \sqrt{(2J+1)}\delta_{JJ'}, \tag{A.11}$$

$$\langle J||\mathbf{J}||J\rangle = \sqrt{J(J+1)(2J+1)}\delta_{JJ'}, \tag{A.12}$$

In the following a tensor space $V = V_1 \bigotimes V_2$ will be considered, where the total angular momentum operator is given by $\mathbf{J} = \mathbf{j_1} + \mathbf{j_2}$. Here, the irreducible tensor operators of rank k_1 on the first space $\mathbf{U}^{(k_1)}$ and of rank k_2 on the second space $\mathbf{V}^{(k_2)}$ give rise to tensor operators of rank k on the tensor space. The rank k of such tensors can range from maximally $k_1 + k_2$ to $|k_1 - k_2|$ as described by the Clebsch-Gordan theorem. This is in complete analogy to the coupling in the basis of the angular momentum states $|(j_1, j_2)J, M\rangle$ in equation A.3. We thus have irreducible tensor operators $T_q^{(k)} = (\mathbf{U}^{(k_1)} \otimes \mathbf{V}^{(k_2)})_q^{(k)}$.

Next a step by step derivation for a formula is shown for reduced matrix elements involving a tensor operator of the shape $T_q^{(k)} = (U_q^{(k)} \otimes \mathbb{1})$. Where the operator acts only non-trivially on the first space and acts with the identity on the second space. If the operator $U_q^{(k)}$ is irreducible on V_1, then the operator $T_q^{(k)}$ is irreducible on V.

$$
\begin{aligned}
\langle J||\mathbf{T}^{(k)}||J'\rangle &= \sum_{M',q} \sqrt{(2J+1)} C^{J,M}_{J',M';k,q} \langle (j_1,j_2)J,M|(U^{(k)}_q \otimes \mathbb{1})|(j_1',j_2')J',M'\rangle \\
&= \sum_{M',q} \sqrt{(2J+1)} C^{J,M}_{J',M';k,q} \sum_{m_1,m_2} C^{J,M}_{j_1,m_1;j_2,m_2} \sum_{m_1',m_2'} C^{J,M}_{j_1',m_1';j_2',m_2'} \\
&\quad \times \langle j_1,m_1;j_2,m_2|(U^{(k)}_q \otimes \mathbb{1})|j_1',m_1';j_2',m_2'\rangle \\
&= \sum_{M',q,m_1,m_2,m_1',m_2'} \sqrt{(2J+1)} C^{J,M}_{J',M';k,q} C^{J,M}_{j_1,m_1;j_2,m_2} C^{J',M'}_{j_1',m_1';j_2',m_2'} \\
&\quad \times \langle j_1,m_1|U^{(k)}_q|j_1',m_1'\rangle \langle j_2,m_2|j_2',m_2'\rangle \\
&= \sum_{M',q,m_1,m_2,m_1',m_2'} \sqrt{(2J+1)} C^{J,M}_{J',M';k,q} C^{J,M}_{j_1,m_1;j_2,m_2} C^{J',M'}_{j_1',m_1';j_2',m_2'} \\
&\quad \times \langle j_1,m_1|U^{(k)}_q|j_1',m_1'\rangle \delta_{j_2,j_2'} \delta_{m_2,m_2'} \\
&= \sum_{M',q,m_1,m_2,m_1'} \sqrt{(2J+1)} C^{J,M}_{J',M';k,q} C^{J,M}_{j_1,m_1;j_2,m_2} C^{J',M'}_{j_1',m_1';j_2,m_2} \\
&\quad \times \langle j_1,m_1|U^{(k)}_q|j_1',m_1'\rangle \delta_{j_2 j_2'} \\
&= \sum_{M',q,m_1,m_2,m_1'} \sqrt{(2J+1)} C^{J,M}_{J',M';k,q} C^{J,M}_{j_1,m_1;j_2,m_2} C^{J',M'}_{j_1',m_1';j_2,m_2} C^{j_1,m_1}_{j_1',m_1';k,q} \\
&\quad \times \frac{1}{\sqrt{(2j_1+1)}} \langle j_1||\mathbf{U}^{(k)}||j_1'\rangle \delta_{j_2 j_2'}
\end{aligned}
$$

In the first step we used the inverse WE theorem A.10, then we expressed the basis elements in the uncoupled basis $|j_1,m_1;j_2,m_2\rangle$. Since this operator is diagonal in the second space, we can omit the sum over m_2' and substitute the j_2',m_2' with the quantities j_2,m_2 in the sum. In the last step we use the WE theorem A.9 in terms of CG-coefficients. The next step is to manipulate the equation to obtain a term that can be expressed as a Wigner 6-j-symbol.

$$
\begin{aligned}
\langle J||\mathbf{T}^{(k)}||J'\rangle = & \sum_{M',q,m_1,m_2,m_1'} \sqrt{(2J+1)}(-1)^{k+J'-J} C^{J,M}_{k,q,J',M'} C^{J,M}_{j_1,m_1;j_2,m_2} \\
& \times (-1)^{2j_1'+J'-m_1'-j_2} \sqrt{\frac{2J'+1}{2j_2+1}} C^{j_2,m_2}_{j_1',-m_1';J',M'} (-1)^{j_1'-m_1'} \\
& \times \sqrt{\frac{2j_1+1}{2k+1}} C^{k,q}_{j_1,m_1;j_1',-m_1'} \frac{1}{\sqrt{(2j_1+1)}} \langle j_1||\mathbf{U}^{(k)}||j_1'\rangle \, \delta_{j_2 j_2'} \\
= & \sum_{M',q,m_1,m_2,m_1'} \sqrt{\frac{(2J+1)(2J'+1)(2j_1+1)}{(2j_2+1)(2k+1)(2j_1+1)}} (-1)^{k+2J'-J+3j_1'-j_2-2m_1'} \\
& \times C^{J,M}_{k,q,J',M'} C^{J,M}_{j_1,m_1;j_2,m_2} C^{j_2,m_2}_{j_1',-m_1';J',M'} C^{k,q}_{j_1,m_1;j_1',-m_1'} \langle j_1||\mathbf{U}^{(k)}||j_1'\rangle \, \delta_{j_2 j_2'} \\
= & \sum_{M',q,m_1,m_2,m_1'} \sqrt{\frac{(2J+1)(2J'+1)}{(2j_2+1)(2k+1)}} (-1)^{k+2J'-J-j_2+j_1'} (-1)^{2(j_1'-m_1')} \\
& \times (-1)^{2(j_1'+j_2'-J')} C^{J,M}_{k,q,J',M'} C^{J,M}_{j_1,m_1;j_2,m_2} C^{j_2,m_2}_{j_1',-m_1';J',M'} C^{k,q}_{j_1,m_1;j_1',-m_1'} \\
& \times \langle j_1||\mathbf{U}^{(k)}||j_1'\rangle \, \delta_{j_2 j_2'} \\
= & \sum_{M',q,m_1,m_2,m_1'} \frac{(-1)^{j_1+j_1'+J'+J}}{\sqrt{(2j_2+1)(2k+1)}} \\
& \qquad \times C^{J,M}_{k,q,J',M'} C^{J,M}_{j_1,m_1;j_2,m_2} C^{j_2,m_2}_{j_1',-m_1';J',M'} C^{k,q}_{j_1,m_1;j_1',-m_1'} \\
& \times (-1)^{j_1+j_2+J'+k} \sqrt{(2J+1)(2J'+1)} \langle j_1||\mathbf{U}^{(k)}||j_1'\rangle \, \delta_{j_2 j_2'} \\
= & \begin{Bmatrix} j_1 & j_1' & k \\ J' & J & j_2 \end{Bmatrix} (-1)^{J'+j_1+j_2+k} \sqrt{(2J+1)(2J'+1)} \langle j_1||\mathbf{U}^{(k)}||j_1'\rangle \, \delta_{j_2 j_2'}
\end{aligned}
$$

First, we used the symmetry relations of the CG-coefficients, yielding extra factors where indices were permuted. After the manipulation, $(j_1, j_1', k, J', J, j_2)$ assume the role of $(j_1, j_2, J_{12}, j_3, J, J_{23})$ in equation A.7 for the 6-j symbol. Additionally we used, that $(j_1' + j_2' - J')$ as well as $(j_1' - m_1')$ are integer numbers, meaning in this case we find for the factors $(-1)^{2(j_1'+j_2-J')} = (-1)^{2(j_1'-m_1')} = 1$. These factors can be multiplied in and out of the equation without changing the value.

Such formulas can be derived for different types of operators. The general formula for an operator $\mathbf{T}^{(k)} = (\mathbf{U}^{(k_1)} \otimes \mathbf{V}^{(k_2)})^{(k)}$ involves a Wigner-9-j symbol, this is beyond what is needed here. The operators considered here are of three types. Operators which only act on one space, such as the one just considered $(U_q^{(k)} \otimes \mathbb{1})$, where the formula was found following the above derivation:

$$\langle (j_1, j_2)J||\mathbf{U}^{(k)} \otimes \mathbb{1}||(j_1', j_2')J'\rangle = (-1)^{J'+j_1+j_2+k}\sqrt{(2J+1)(2J'+1)} \times \begin{Bmatrix} j_1 & k & j_1' \\ J' & j_2 & J \end{Bmatrix} \langle j_1||\mathbf{U}^{(k)}||j_1'\rangle\, \delta_{j_2 j_2'}, \tag{A.13}$$

Equivalently we can consider the case, of a tensor operator only acting on the second space. This means we have an operator $(\mathbb{1} \otimes V_q^{(k)})$. The same way as for equation A.13 we can express a reduced matrix element of such an operator as:

$$\langle (j_1, j_2)J||\mathbb{1} \otimes \mathbf{V}^{(k)}||(j_1', j_2')J'\rangle = (-1)^{J+j_1+j_2'+k}\sqrt{(2J+1)(2J'+1)} \times \begin{Bmatrix} j_2 & k & j_2' \\ J' & j_1 & J \end{Bmatrix} \langle j_2||\mathbf{V}^{(k)}||j_2'\rangle\, \delta_{j_1 j_1'}, \tag{A.14}$$

The other type of operator that is recurrent is $(\mathbf{U}^{(k)} \otimes \mathbf{V}^{(k)})_0^{(0)}$, these are the rank zero irreducible tensor operators that we have, when considering the tensor product between two tensors of the same rank k. Often we refer to these as the scalar product and use the notation $(\mathbf{U} \cdot \mathbf{V})$ to denote these tensors. Reduced matrix elements involving such operators can be expressed as:

$$\langle (j_1, j_2)J||(\mathbf{U}^{(k)} \otimes \mathbf{V}^{(k)})^{(0)}||(j_1', j_2')J'\rangle = (-1)^{J+j_1'+j_2}\sqrt{(2J+1)} \times \begin{Bmatrix} j_1 & k & j_1' \\ j_2' & J & j_2 \end{Bmatrix} \langle j_1||\mathbf{U}^{(k)}||j_1'\rangle\, \langle j_2||\mathbf{V}^{(k)}||j_2'\rangle\, \delta_{JJ'}, \tag{A.15}$$

All the equations are derived following the same procedure, using the WE equation A.9, the inverse A.10 and writing the states in the uncoupled basis A.3. We see that they share similarities, for that reason we have to be careful with the labeling, denoting j_1 and j_2 consistently and noting when we have primed quantities.

Appendix B

Eigenstate labels

Here are the state labels i used for the lowest four rotational states L. On the first page the tables on the left column show the two para-H_2^+ levels $L = 0, 2$. The right column shows the ortho-H_2^+ level $L = 1$. On a second page the level $L = 3$ is shown in two columns. As we can see, the number of states rapidly increases with L and we have more states for ortho-H_2^+ level than for para-H_2^+ levels of a similar rotational level L.

Rotational Level $L = 0$

i	F	J	M_J
0	$\frac{1}{2}$	$\frac{1}{2}$	$-\frac{1}{2}$
1	$\frac{1}{2}$	$\frac{1}{2}$	$+\frac{1}{2}$

Rotational Level $L = 1$

i	F	J	M_J
0	$\frac{1}{2}$	$\frac{1}{2}$	$-\frac{1}{2}$
1	$\frac{1}{2}$	$\frac{1}{2}$	$+\frac{1}{2}$
2	$\frac{1}{2}$	$\frac{3}{2}$	$-\frac{3}{2}$
3	$\frac{1}{2}$	$\frac{3}{2}$	$-\frac{1}{2}$
4	$\frac{1}{2}$	$\frac{3}{2}$	$+\frac{1}{2}$
5	$\frac{1}{2}$	$\frac{3}{2}$	$+\frac{3}{2}$
6	$\frac{3}{2}$	$\frac{1}{2}$	$-\frac{1}{2}$
7	$\frac{3}{2}$	$\frac{1}{2}$	$+\frac{1}{2}$
8	$\frac{3}{2}$	$\frac{3}{2}$	$-\frac{3}{2}$
9	$\frac{3}{2}$	$\frac{3}{2}$	$-\frac{1}{2}$
10	$\frac{3}{2}$	$\frac{3}{2}$	$+\frac{1}{2}$
11	$\frac{3}{2}$	$\frac{3}{2}$	$+\frac{3}{2}$
12	$\frac{3}{2}$	$\frac{5}{2}$	$-\frac{5}{2}$
13	$\frac{3}{2}$	$\frac{5}{2}$	$-\frac{3}{2}$
14	$\frac{3}{2}$	$\frac{5}{2}$	$-\frac{1}{2}$
15	$\frac{3}{2}$	$\frac{5}{2}$	$+\frac{1}{2}$
16	$\frac{3}{2}$	$\frac{5}{2}$	$+\frac{3}{2}$
17	$\frac{3}{2}$	$\frac{5}{2}$	$+\frac{5}{2}$

Rotational Level $L = 2$

i	F	J	M_J
0	$\frac{1}{2}$	$\frac{3}{2}$	$-\frac{3}{2}$
1	$\frac{1}{2}$	$\frac{3}{2}$	$-\frac{1}{2}$
2	$\frac{1}{2}$	$\frac{3}{2}$	$+\frac{1}{2}$
3	$\frac{1}{2}$	$\frac{3}{2}$	$+\frac{3}{2}$
4	$\frac{1}{2}$	$\frac{5}{2}$	$-\frac{5}{2}$
5	$\frac{1}{2}$	$\frac{5}{2}$	$-\frac{3}{2}$
6	$\frac{1}{2}$	$\frac{5}{2}$	$-\frac{1}{2}$
7	$\frac{1}{2}$	$\frac{5}{2}$	$+\frac{1}{2}$
8	$\frac{1}{2}$	$\frac{5}{2}$	$+\frac{3}{2}$
9	$\frac{1}{2}$	$\frac{5}{2}$	$+\frac{5}{2}$

Rotational Level $L = 3$

i	F	J	M_J
0	$\frac{1}{2}$	$\frac{5}{2}$	$-\frac{5}{2}$
1	$\frac{1}{2}$	$\frac{5}{2}$	$-\frac{3}{2}$
2	$\frac{1}{2}$	$\frac{5}{2}$	$-\frac{1}{2}$
3	$\frac{1}{2}$	$\frac{5}{2}$	$+\frac{1}{2}$
4	$\frac{1}{2}$	$\frac{5}{2}$	$+\frac{3}{2}$
5	$\frac{1}{2}$	$\frac{5}{2}$	$+\frac{5}{2}$
6	$\frac{1}{2}$	$\frac{7}{2}$	$-\frac{7}{2}$
7	$\frac{1}{2}$	$\frac{7}{2}$	$-\frac{5}{2}$
8	$\frac{1}{2}$	$\frac{7}{2}$	$-\frac{3}{2}$
9	$\frac{1}{2}$	$\frac{7}{2}$	$-\frac{1}{2}$
10	$\frac{1}{2}$	$\frac{7}{2}$	$+\frac{1}{2}$
11	$\frac{1}{2}$	$\frac{7}{2}$	$+\frac{3}{2}$
12	$\frac{1}{2}$	$\frac{7}{2}$	$+\frac{5}{2}$
13	$\frac{1}{2}$	$\frac{7}{2}$	$+\frac{7}{2}$
14	$\frac{3}{2}$	$\frac{3}{2}$	$-\frac{3}{2}$
15	$\frac{3}{2}$	$\frac{3}{2}$	$-\frac{1}{2}$
16	$\frac{3}{2}$	$\frac{3}{2}$	$+\frac{1}{2}$
17	$\frac{3}{2}$	$\frac{3}{2}$	$+\frac{3}{2}$
18	$\frac{3}{2}$	$\frac{5}{2}$	$-\frac{5}{2}$
19	$\frac{3}{2}$	$\frac{5}{2}$	$-\frac{3}{2}$
20	$\frac{3}{2}$	$\frac{5}{2}$	$-\frac{1}{2}$

i	F	J	M_J
21	$\frac{3}{2}$	$\frac{5}{2}$	$+\frac{1}{2}$
22	$\frac{3}{2}$	$\frac{5}{2}$	$+\frac{3}{2}$
23	$\frac{3}{2}$	$\frac{5}{2}$	$+\frac{5}{2}$
24	$\frac{3}{2}$	$\frac{7}{2}$	$-\frac{7}{2}$
25	$\frac{3}{2}$	$\frac{7}{2}$	$-\frac{5}{2}$
26	$\frac{3}{2}$	$\frac{7}{2}$	$-\frac{3}{2}$
27	$\frac{3}{2}$	$\frac{7}{2}$	$-\frac{1}{2}$
28	$\frac{3}{2}$	$\frac{7}{2}$	$+\frac{1}{2}$
29	$\frac{3}{2}$	$\frac{7}{2}$	$+\frac{3}{2}$
30	$\frac{3}{2}$	$\frac{7}{2}$	$+\frac{5}{2}$
31	$\frac{3}{2}$	$\frac{7}{2}$	$+\frac{7}{2}$
32	$\frac{3}{2}$	$\frac{9}{2}$	$-\frac{9}{2}$
33	$\frac{3}{2}$	$\frac{9}{2}$	$-\frac{7}{2}$
34	$\frac{3}{2}$	$\frac{9}{2}$	$-\frac{5}{2}$
35	$\frac{3}{2}$	$\frac{9}{2}$	$-\frac{3}{2}$
36	$\frac{3}{2}$	$\frac{9}{2}$	$-\frac{1}{2}$
37	$\frac{3}{2}$	$\frac{9}{2}$	$+\frac{1}{2}$
38	$\frac{3}{2}$	$\frac{9}{2}$	$+\frac{3}{2}$
39	$\frac{3}{2}$	$\frac{9}{2}$	$+\frac{5}{2}$
40	$\frac{3}{2}$	$\frac{9}{2}$	$+\frac{7}{2}$
41	$\frac{3}{2}$	$\frac{9}{2}$	$+\frac{9}{2}$

Appendix C

Transition probabilities

C.1 Magnetic Dipole Transitions (M1)

Tables for magnetic field insensitive (M1) transitions in the 1 mT range for ground vibrational ($\nu = 0$) and the four lowest rotational levels ($L = 0, 1, 2, 3$). For the para-H_2^+ groundstate, there are no insensitive transitions, as there are only two levels, which are pure. Only the matrix element is shown with the polarization q, which could have a non-zero value according to equation 4.3. The tree standard polarizations are right-hand circular σ_+ ($q = 1$), linear π ($q = 0$) and left-hand circular σ_- ($q = -1$).

$(\nu, L) = (0, 1)$							
i	M_J	f	M'_J	B [μT]	q	$\lvert \langle f \rvert \mu_q/\mu_b \lvert i \rangle \rvert$	f_{hf} [MHz]
6	$-\frac{1}{2}$	13	$-\frac{3}{2}$	15.29	-1	0.00544	88.7101
9	$-\frac{1}{2}$	14	$-\frac{1}{2}$	44.93	0	0.38639	7.8314
4	$+\frac{1}{2}$	9	$-\frac{1}{2}$	175.67	-1	0.4452	1412.1348
1	$+\frac{1}{2}$	3	$-\frac{1}{2}$	197.74	-1	0.20322	19.5997
8	$-\frac{3}{2}$	13	$-\frac{3}{2}$	202.17	0	0.32553	7.6292
1	$+\frac{1}{2}$	15	$+\frac{1}{2}$	233.38	0	0.15604	1384.9864
3	$-\frac{1}{2}$	15	$+\frac{1}{2}$	277.94	1	0.52651	1404.5916
6	$-\frac{1}{2}$	8	$-\frac{3}{2}$	334.1	-1	0.55286	96.2111
0	$-\frac{1}{2}$	9	$-\frac{1}{2}$	458.26	0	0.6635	1392.0777
10	$+\frac{1}{2}$	16	$+\frac{3}{2}$	468.05	1	0.28497	6.8241
9	$-\frac{1}{2}$	15	$+\frac{1}{2}$	488.55	1	0.22034	6.4608
0	$-\frac{1}{2}$	15	$+\frac{1}{2}$	509.73	1	0.21337	1385.6197
3	$-\frac{1}{2}$	9	$-\frac{1}{2}$	538.93	0	0.55052	1410.9949
0	$-\frac{1}{2}$	3	$-\frac{1}{2}$	600.44	0	0.32637	18.8975
7	$+\frac{1}{2}$	10	$+\frac{1}{2}$	763.84	0	0.43913	94.9703
8	$-\frac{3}{2}$	14	$-\frac{1}{2}$	787.96	1	0.14017	5.2398

$(\nu, L) = (0, 2)$							
i	M_J	f	M'_J	B [μT]	q	$\lvert \langle f \rvert \mu_q/\mu_b \lvert i \rangle \rvert$	f_{hf} [MHz]
2	$+\frac{1}{2}$	6	$-\frac{1}{2}$	0.42	-1	0.69372	105.4088
1	$-\frac{1}{2}$	7	$+\frac{1}{2}$	2.38	1	0.69424	105.4088
1	$-\frac{1}{2}$	6	$-\frac{1}{2}$	752.06	0	1.00141	103.2791

$(\nu, L) = (0, 3)$							
i	M_J	f	M'_J	B [μT]	q	$\lvert \langle f \rvert \mu_q/\mu_b \lvert i \rangle \rvert$	f_{hf} [MHz]
19	$-\frac{3}{2}$	27	$-\frac{1}{2}$	22.86	1	0.30887	65.8919
27	$-\frac{1}{2}$	36	$-\frac{1}{2}$	44.13	0	0.45985	17.724
4	$+\frac{3}{2}$	28	$+\frac{1}{2}$	44.13	-1	0.31113	1384.0982
19	$-\frac{3}{2}$	36	$-\frac{1}{2}$	52.81	1	0.00419	83.6152
1	$-\frac{3}{2}$	36	$-\frac{1}{2}$	102.3	1	0.00688	1401.8046
3	$+\frac{1}{2}$	21	$+\frac{1}{2}$	122.54	0	0.18765	1318.2071
10	$+\frac{1}{2}$	36	$-\frac{1}{2}$	125.79	-1	0.59603	1448.2218
26	$-\frac{3}{2}$	35	$-\frac{3}{2}$	144.22	0	0.43867	17.6629
31	$+\frac{7}{2}$	39	$+\frac{5}{2}$	178.25	-1	0.09498	17.6537
20	$-\frac{1}{2}$	36	$-\frac{1}{2}$	238.47	0	0.0375	83.49
3	$+\frac{1}{2}$	9	$-\frac{1}{2}$	246.43	-1	0.22139	-46.3899
4	$+\frac{3}{2}$	22	$+\frac{3}{2}$	248.33	0	0.53857	1318.2241
30	$+\frac{5}{2}$	38	$+\frac{3}{2}$	248.36	-1	0.16107	17.5471
2	$-\frac{1}{2}$	36	$-\frac{1}{2}$	281.99	0	0.03749	1401.6621
25	$-\frac{5}{2}$	34	$-\frac{5}{2}$	281.99	0	0.39219	17.5053
5	$+\frac{5}{2}$	23	$+\frac{5}{2}$	281.99	0	0.86662	1318.2428
3	$+\frac{1}{2}$	28	$+\frac{1}{2}$	305.55	0	0.62082	1384.225
9	$-\frac{1}{2}$	21	$+\frac{1}{2}$	305.55	1	0.22671	1364.5896
29	$+\frac{3}{2}$	37	$+\frac{1}{2}$	315.57	-1	0.22416	17.3975
8	$-\frac{3}{2}$	15	$-\frac{1}{2}$	345.98	1	0.00799	1282.6326
21	$+\frac{1}{2}$	28	$+\frac{1}{2}$	360.42	0	0.60964	66.032
9	$-\frac{1}{2}$	36	$-\frac{1}{2}$	393.1	0	0.89005	1447.809
28	$+\frac{1}{2}$	36	$-\frac{1}{2}$	401.72	-1	0.28407	17.1832
21	$+\frac{1}{2}$	36	$-\frac{1}{2}$	417.05	-1	0.04373	83.2131

Continued on next page

$(\nu, L) = (0, 3)$							
i	M_J	f	M'_J	B [μT]	q	$\lvert \langle f \rvert \mu_q/\mu_b \lvert i \rangle \rvert$	f_{hf} [MHz]
3	$+\frac{1}{2}$	36	$-\frac{1}{2}$	463.57	-1	0.04181	1401.3893
18	$-\frac{5}{2}$	35	$-\frac{3}{2}$	467.88	1	0.02143	83.0336
9	$-\frac{1}{2}$	28	$+\frac{1}{2}$	480.97	1	0.51594	1430.6271
27	$-\frac{1}{2}$	35	$-\frac{3}{2}$	520.22	-1	0.33974	16.8562
24	$-\frac{7}{2}$	33	$-\frac{7}{2}$	549.42	0	0.30583	17.1056
2	$-\frac{1}{2}$	28	$+\frac{1}{2}$	607.76	1	0.46221	1384.5573
15	$-\frac{1}{2}$	36	$-\frac{1}{2}$	629.46	0	0.00008	164.3518
2	$-\frac{1}{2}$	9	$-\frac{1}{2}$	642.98	0	0.33097	-46.0636
0	$-\frac{5}{2}$	35	$-\frac{3}{2}$	680.54	1	0.02469	1400.8946
8	$-\frac{3}{2}$	36	$-\frac{1}{2}$	694.96	1	0.62228	1446.9227
26	$-\frac{3}{2}$	34	$-\frac{5}{2}$	719.49	-1	0.38605	16.2973
19	$-\frac{3}{2}$	35	$-\frac{3}{2}$	759.87	0	0.10216	82.3805
3	$+\frac{1}{2}$	15	$-\frac{1}{2}$	855.54	-1	0.55843	1237.1638
4	$+\frac{3}{2}$	23	$+\frac{5}{2}$	855.54	1	0.4908	1318.6191
20	$-\frac{1}{2}$	28	$+\frac{1}{2}$	889.0	1	0.47279	66.531
9	$-\frac{1}{2}$	20	$-\frac{1}{2}$	932.27	0	0.3204	1364.0673
1	$-\frac{3}{2}$	35	$-\frac{3}{2}$	974.52	0	0.10385	1400.1867
3	$+\frac{1}{2}$	22	$+\frac{3}{2}$	992.92	1	0.6363	1318.6607

C.2 Two-photon Transitions (2E1)

Here we only consider the case of driving the two-photon transitions with one laser of a certain polarization q. This leads to transitions for which $|\Delta M_J| = 0, 2$. Polarization is adjusted according to the transition, linear for $\Delta M_J = 0$ and circular for $|\Delta M_J| = 2$. We could in principle also drive transitions with $|\Delta M_J| = 1$, but we would need two lasers of different polarizations.

The frequency shifts in the table C.2 are for the full transition, if we want to calculate the shift for each of the two photons, we have to take half of each value respectively. Here we have chosen the propagation direction of the photons to be along the quantization axis, therefore the polarizabilities that are used are $\alpha_{\parallel}$. If we were to position the laser at an angle θ from the axis we would have to use α_{θ}, which would in general lead to a different light shift Δf_{LS}.

$(\nu, L) = (0, 1)$		$(\nu', L') = (1, 1)$						$f_0 = 65596427.538167596$ MHz	
i	M_J	f	M'_J	B [μT]	$\Delta\alpha_{if}$	q	$\lvert \langle f \rvert {}^S Q_{qq} \lvert i \rangle \rvert$	Δf_{hf} [MHz]	Δf_{LS} [Hz]
8	$-\frac{3}{2}$	8	$-\frac{3}{2}$	3.09	0.91355	0	0.51213	-13.428	-4.46
9	$-\frac{1}{2}$	9	$-\frac{1}{2}$	10.4	0.55	0	0.32697	-13.428	-4.205
14	$-\frac{1}{2}$	14	$-\frac{1}{2}$	16.43	0.91355	0	0.5144	-12.8484	-4.44
15	$+\frac{1}{2}$	15	$+\frac{1}{2}$	16.63	0.91355	0	0.51113	-12.8484	-4.468
10	$+\frac{1}{2}$	10	$+\frac{1}{2}$	19.1	0.55	0	0.3297	-13.428	-4.17
13	$-\frac{3}{2}$	13	$-\frac{3}{2}$	24.17	0.77722	0	0.44829	-12.8485	-4.334
16	$+\frac{3}{2}$	16	$+\frac{3}{2}$	25.45	0.77722	0	0.43845	-12.8485	-4.432
14	$-\frac{1}{2}$	9	$-\frac{1}{2}$	43.5	-0.30691	0	0.06292	-5.5959	12.195
9	$-\frac{1}{2}$	14	$-\frac{1}{2}$	43.87	1.77046	0	0.06489	-20.6803	-68.206
11	$+\frac{3}{2}$	11	$+\frac{3}{2}$	47.71	0.91355	0	0.52201	-13.428	-4.375
3	$-\frac{1}{2}$	3	$-\frac{1}{2}$	53.83	0.959	0	0.53178	24.6475	-4.508
4	$+\frac{1}{2}$	4	$+\frac{1}{2}$	105.61	0.959	0	0.54359	24.6475	-4.41
2	$-\frac{3}{2}$	10	$+\frac{1}{2}$	164.72	0.65711	1	0.00514	1398.7492	-319.746
2	$-\frac{3}{2}$	2	$-\frac{3}{2}$	169.45	0.50456	0	0.30481	24.6463	-4.138
10	$+\frac{1}{2}$	2	$-\frac{3}{2}$	175.84	0.39744	-1	0.00515	-1387.5224	-193.058
13	$-\frac{3}{2}$	8	$-\frac{3}{2}$	194.28	1.23489	0	0.16876	-5.7885	-18.294

Continued on next page

$(\nu, L) = (0, 1)$		$(\nu', L') = (1, 1)$						$f_0 = 65596427.538167596$ MHz	
i	M_J	f	M'_J	B [μT]	$\Delta\alpha_{if}$	q	$\lvert \langle f \rvert {}^S Q_{qq} \lvert i \rangle \rvert$	Δf_{hf} [MHz]	Δf_{LS} [Hz]
8	$-\frac{3}{2}$	13	$-\frac{3}{2}$	195.17	0.45588	0	0.17772	-20.4861	-6.413
1	$+\frac{1}{2}$	15	$+\frac{1}{2}$	219.94	1.342	0	0.00535	1372.1244	-627.091
15	$+\frac{1}{2}$	1	$+\frac{1}{2}$	227.86	0.30332	0	0.00516	-1361.4709	-147.043
0	$-\frac{1}{2}$	0	$-\frac{1}{2}$	287.23	0.73178	0	0.44306	23.5041	-4.129
5	$+\frac{3}{2}$	14	$-\frac{1}{2}$	309.17	1.87757	-1	0.00055	1391.9189	-8559.564
14	$-\frac{1}{2}$	5	$+\frac{3}{2}$	335.31	-0.45946	1	0.00049	-1380.1448	2321.653
0	$-\frac{1}{2}$	9	$-\frac{1}{2}$	411.13	0.12155	0	0.00295	1378.7037	-103.061
9	$-\frac{1}{2}$	0	$-\frac{1}{2}$	470.61	1.16023	0	0.00295	-1368.5697	-981.825
3	$-\frac{1}{2}$	9	$-\frac{1}{2}$	513.05	-0.41402	0	0.00262	1397.6396	394.57
9	$-\frac{1}{2}$	3	$-\frac{1}{2}$	529.47	1.92302	0	0.00305	-1386.3689	-1577.497
0	$-\frac{1}{2}$	3	$-\frac{1}{2}$	582.66	1.49456	0	0.16869	5.7237	-22.15
3	$-\frac{1}{2}$	0	$-\frac{1}{2}$	590.9	0.19621	0	0.17723	42.4112	-2.768
6	$-\frac{1}{2}$	6	$-\frac{1}{2}$	649.29	0.73178	0	0.41496	-7.3962	-4.409
7	$+\frac{1}{2}$	10	$+\frac{1}{2}$	723.47	0.12155	0	0.101	81.6407	-3.009
10	$+\frac{1}{2}$	7	$+\frac{1}{2}$	746.21	1.16023	0	0.10199	-102.4098	-28.44
12	$-\frac{5}{2}$	12	$-\frac{5}{2}$	1000	0.50456	0	0.30476	-12.8484	-4.139

Continued on next page

$(\nu, L) = (0, 1)$		$(\nu', L') = (1, 1)$						$f_0 = 65596427.538167596$ MHz	
i	M_J	f	M'_J	B [μT]	$\Delta\alpha_{if}$	q	$\lvert \langle f \rvert {}^S Q_{qq} \lvert i \rangle \rvert$	Δf_{hf} [MHz]	Δf_{LS} [Hz]
17	$+\frac{5}{2}$	17	$+\frac{5}{2}$	1000	0.50456	0	0.30476	-12.8483	-4.139

Table C.2: Magnetic field insensitive (2E1) transitions in the 1 mT range between hyperfine states of the ortho-groundstate and the first excited vibrational level, when driving with one laser of polarization q along the quantization axis. The magnetic field value is indicated at which the transition is insensitive. Together with the difference of the static polarizabilities of the two states $\Delta\alpha_{if}$, the polarization of the laser light q and the corresponding matrix element of the two-photon transition operator. Then the frequency shift of the transition frequencies is indicated. First is the hyperfine frequency Δf_{hf} due to the effective spin Hamiltonian, lastly the light shift due to the driving laser Δf_{LS} is indicated. Note that in contrast to the other frequencies (given in MHz), this frequency is given in Hz.

C.3 Electric Quadrupole Transitions (E2)

Here we display magnetic field insensitive electric quadrupole (E2) transitions in the 1 mT range between different ro-vibrational levels.

We indicate the initial $|i\rangle$ and final $|f\rangle$ states, together with the quantum number M_J corresponding to the projection of the total angular momentum onto the quantization axis. Additionally the magnetic field strength B at which the transition is insensitive, the difference in the static polarizability between the two states $\Delta\alpha_\theta$ (where the anlge θ is given by the propagation direction $\vec{n}$) and the matrix element $|\Theta^{if}_{\epsilon,n}|$ as defined in equation 4.11 are given. The chosen polarization and propagation vectors, depending on the $|\Delta M_J|$ of the transition, are:

$$\vec{\epsilon}_{\pm 2} = \hat{e}_y, \qquad \vec{n}_{\pm 2} = \sin\frac{\pi}{2}\hat{e}_x + \cos\frac{\pi}{2}\hat{e}_z,$$
$$\vec{\epsilon}_{\pm 1} = \hat{e}_z, \qquad \vec{n}_{\pm 1} = \hat{e}_x,$$
$$\vec{\epsilon}_0 = \cos\frac{\pi}{4}\hat{e}_x - \sin\frac{\pi}{4}\hat{e}_z, \qquad \vec{n}_0 = \sin\frac{\pi}{4}\hat{e}_x + \cos\frac{\pi}{4}\hat{e}_z,$$

Finally both the hyperfine frequency shift from the effective spin Hamiltonian and the light shift are given. Note that the light shift is intensity dependent, for the weakest transitions, with $|\Theta^{if}_{\epsilon,n}| \leq 10^{-5}$, to achieve a π-pulse we need a very large intensity, witch experimentally is not feasible and thus this transition is not really relevant.

$(\nu, L) = (0, 1)$		$(\nu', L') = (3, 3)$					$f_0 = 192818042.8465861$ MHz	
i	M_J	f	M'_J	B [μT]	$\Delta\alpha_{if}$	$\lvert\Theta^{if}_{\epsilon,n}\rvert$	Δf_{hf} [MHz]	Δf_{LS} [Hz]
15	$+\frac{1}{2}$	15	$-\frac{1}{2}$	0.7	2.57424	0.2504(-4)	-144.7496	-2142.605
14	$-\frac{1}{2}$	16	$+\frac{1}{2}$	3.7	2.57424	0.2504(-4)	-144.7496	-2142.632
10	$+\frac{1}{2}$	29	$+\frac{3}{2}$	14.36	2.39077	2.1167(-4)	-31.3203	-27.857
0	$-\frac{1}{2}$	10	$+\frac{1}{2}$	35.13	2.06458	0.0082(-4)	40.2109	-1595333.356
6	$-\frac{1}{2}$	17	$+\frac{3}{2}$	47.52	3.57054	2.7228(-4)	-56.0391	-25.142
13	$-\frac{3}{2}$	24	$-\frac{7}{2}$	57.62	3.85948	1.3929(-4)	-23.4788	-103.842
9	$-\frac{1}{2}$	16	$+\frac{1}{2}$	62.85	2.14578	0.0156(-4)	-152.5749	-459549.322
16	$+\frac{3}{2}$	39	$+\frac{5}{2}$	73.86	2.80867	2.7071(-4)	-8.4567	-20.007
15	$+\frac{1}{2}$	8	$-\frac{3}{2}$	74.75	2.63909	0.0525(-4)	-1344.5781	-49968.31
15	$+\frac{1}{2}$	37	$+\frac{1}{2}$	97.03	3.27848	3.0736(-4)	-8.4939	-18.116
15	$+\frac{1}{2}$	5	$+\frac{5}{2}$	105.78	4.26033	0.0391(-4)	-1306.0743	-145769.554
9	$-\frac{1}{2}$	11	$+\frac{3}{2}$	117.69	2.21063	0.0132(-4)	-1352.343	-666113.441
15	$+\frac{1}{2}$	23	$+\frac{5}{2}$	146.03	3.77396	0.8073(-4)	-77.9496	-302.301
11	$+\frac{3}{2}$	40	$+\frac{7}{2}$	146.47	3.59982	0.3158(-4)	-16.2572	-1883.786
14	$-\frac{1}{2}$	35	$-\frac{3}{2}$	149.55	2.54902	2.5159(-4)	-8.572	-21.023
1	$+\frac{1}{2}$	22	$+\frac{3}{2}$	151.62	2.84638	0.0852(-4)	1306.9022	-20454.896

Continued on next page

$(\nu, L) = (0, 1)$		$(\nu', L') = (3, 3)$					$f_0 = 192818042.8465861$ MHz	
i	M_J	f	M'_J	B [μT]	$\Delta\alpha_{if}$	$\lvert\Theta^{if}_{\epsilon,n}\rvert$	Δf_{hf} [MHz]	Δf_{LS} [Hz]
3	$-\frac{1}{2}$	4	$+\frac{3}{2}$	154.02	3.01689	1.1282(-4)	98.3796	-123.733
9	$-\frac{1}{2}$	18	$-\frac{5}{2}$	161.53	3.3455	2.1032(-4)	-85.6148	-39.482
9	$-\frac{1}{2}$	0	$-\frac{5}{2}$	180.96	3.83188	0.0945(-4)	-1313.7495	-22422.053
14	$-\frac{1}{2}$	26	$-\frac{3}{2}$	194.21	2.81922	0.204(-4)	-23.5568	-3535.606
9	$-\frac{1}{2}$	27	$-\frac{1}{2}$	206.13	3.37262	2.284(-4)	-31.0888	-33.75
15	$+\frac{1}{2}$	4	$+\frac{3}{2}$	218.12	2.96334	0.0242(-4)	-1306.2004	-264476.487
3	$-\frac{1}{2}$	22	$+\frac{3}{2}$	249.78	3.11417	0.0335(-4)	1326.4969	-144975.728
8	$-\frac{3}{2}$	24	$-\frac{7}{2}$	257.12	4.02015	2.9713(-4)	-31.0648	-23.77
10	$+\frac{1}{2}$	30	$+\frac{5}{2}$	260.4	2.87114	1.4513(-4)	-30.9957	-71.161
15	$+\frac{1}{2}$	22	$+\frac{3}{2}$	265.96	3.06061	0.3828(-4)	-78.0942	-1090.317
9	$-\frac{1}{2}$	19	$-\frac{3}{2}$	274.78	2.63216	0.2594(-4)	-85.4263	-2042.295
9	$-\frac{1}{2}$	10	$+\frac{1}{2}$	285.12	1.85036	0.0166(-4)	-1352.0316	-352289.894
0	$-\frac{1}{2}$	20	$-\frac{1}{2}$	296.7	3.20306	0.0958(-4)	1306.9548	-18209.161
9	$-\frac{1}{2}$	1	$-\frac{3}{2}$	307.08	2.53488	0.012(-4)	-1313.5427	-918373.995
13	$-\frac{3}{2}$	33	$-\frac{7}{2}$	321.55	3.43915	2.7349(-4)	-8.8378	-24.003
15	$+\frac{1}{2}$	3	$+\frac{1}{2}$	348.44	3.29049	0.049(-4)	-1306.4201	-71423.576

Continued on next page

$(\nu, L) = (0, 1)$		$(\nu', L') = (3, 3)$					$f_0 = 192818042.8465861$ MHz	
i	M_J	f	M'_J	B [μT]	$\Delta\alpha_{if}$	$\lvert\Theta^{if}_{\epsilon,n}\rvert$	Δf_{hf} [MHz]	Δf_{LS} [Hz]
1	$+\frac{1}{2}$	4	$+\frac{3}{2}$	349.92	2.74911	2.8792(-4)	78.7918	-17.312
15	$+\frac{1}{2}$	36	$-\frac{1}{2}$	370.44	2.33886	2.1022(-4)	-9.2001	-27.627
3	$-\frac{1}{2}$	36	$-\frac{1}{2}$	399.93	3.2517	0.0129(-4)	1395.3775	-1024829.002
3	$-\frac{1}{2}$	3	$+\frac{1}{2}$	400.89	2.36839	0.9281(-4)	98.1605	-143.535
9	$-\frac{1}{2}$	20	$-\frac{1}{2}$	409.99	3.31017	1.2901(-4)	-85.139	-103.83
4	$+\frac{1}{2}$	35	$-\frac{3}{2}$	410.03	2.60257	0.0057(-4)	1395.4076	-4115002.425
15	$+\frac{1}{2}$	21	$+\frac{1}{2}$	410.05	3.09594	0.9456(-4)	-78.3338	-180.733
1	$+\frac{1}{2}$	23	$+\frac{5}{2}$	417.82	3.55973	0.1002(-4)	1307.0979	-18517.038
16	$+\frac{3}{2}$	38	$+\frac{3}{2}$	442.31	3.25374	2.7407(-4)	-9.2026	-22.613
1	$+\frac{1}{2}$	15	$-\frac{1}{2}$	454.24	2.36001	0.0941(-4)	1240.4524	-13912.027
9	$-\frac{1}{2}$	2	$-\frac{1}{2}$	462.06	3.50472	0.0569(-4)	-1313.2222	-56540.074
14	$-\frac{1}{2}$	34	$-\frac{5}{2}$	474.09	2.96934	1.9799(-4)	-9.551	-39.543
9	$-\frac{1}{2}$	28	$+\frac{1}{2}$	479.98	2.15059	0.9357(-4)	-30.2695	-128.23
0	$-\frac{1}{2}$	2	$-\frac{1}{2}$	479.98	3.39761	3.0986(-4)	78.8556	-18.473
9	$-\frac{1}{2}$	9	$-\frac{1}{2}$	488.69	3.52273	0.0313(-4)	-1351.4315	-188067.235
15	$+\frac{1}{2}$	9	$-\frac{1}{2}$	498.81	2.27881	0.0361(-4)	-1344.9707	-91086.366

Continued on next page

$(\nu, L) = (0, 1)$		$(\nu', L') = (3, 3)$					$f_0 = 192818042.8465861$ MHz	
i	M_J	f	M'_J	B [μT]	$\Delta\alpha_{if}$	$\lvert\Theta^{if}_{\epsilon,n}\rvert$	Δf_{hf} [MHz]	Δf_{LS} [Hz]
0	$-\frac{1}{2}$	28	$+\frac{1}{2}$	501.07	2.36481	0.0018(-4)	1361.8099	-38364081.771
0	$-\frac{1}{2}$	9	$-\frac{1}{2}$	519.5	3.41562	0.193(-4)	40.6494	-4785.826
15	$+\frac{1}{2}$	2	$-\frac{1}{2}$	519.5	2.31484	0.024(-4)	-1306.765	-209049.4
3	$-\frac{1}{2}$	21	$+\frac{1}{2}$	534.38	2.75749	0.0261(-4)	1326.2192	-211184.323
15	$+\frac{1}{2}$	28	$+\frac{1}{2}$	542.58	3.15839	0.9372(-4)	-23.8103	-187.728
9	$-\frac{1}{2}$	21	$+\frac{1}{2}$	544.97	2.27548	1.586(-4)	-84.7756	-47.226
1	$+\frac{1}{2}$	8	$-\frac{3}{2}$	545.91	2.42486	0.0722(-4)	40.6039	-24270.002
8	$-\frac{3}{2}$	25	$-\frac{5}{2}$	569.57	3.29959	1.5629(-4)	-30.0894	-70.515
10	$+\frac{1}{2}$	14	$-\frac{3}{2}$	587.05	3.35631	1.1587(-4)	-151.2893	-130.498
2	$-\frac{3}{2}$	37	$+\frac{1}{2}$	618.52	1.85685	0.0033(-4)	1395.0036	-8819040.15
3	$-\frac{1}{2}$	2	$-\frac{1}{2}$	645.55	3.26371	0.391(-4)	97.7416	-1114.674
15	$+\frac{1}{2}$	20	$-\frac{1}{2}$	650.55	2.70394	0.649(-4)	-78.7298	-335.135
9	$-\frac{1}{2}$	22	$+\frac{3}{2}$	657.12	2.63216	1.3568(-4)	-84.3816	-74.644
9	$-\frac{1}{2}$	3	$+\frac{1}{2}$	657.12	1.88638	0.0694(-4)	-1312.7791	-20434.7
9	$-\frac{1}{2}$	15	$-\frac{1}{2}$	671.02	3.37502	0.8892(-4)	-150.6737	-222.809
0	$-\frac{1}{2}$	21	$+\frac{1}{2}$	682.47	2.48971	0.074(-4)	1307.3343	-23711.381

Continued on next page

$(\nu, L) = (0, 1)$		$(\nu', L') = (3, 3)$					$f_0 = 192818042.8465861$ MHz	
i	M_J	f	M'_J	B [μT]	$\Delta\alpha_{if}$	$\lvert\Theta^{if}_{\epsilon,n}\rvert$	Δf_{hf} [MHz]	Δf_{LS} [Hz]
7	$+\frac{1}{2}$	38	$+\frac{3}{2}$	722.68	2.33479	0.0152(-4)	78.9851	-528959.58
9	$-\frac{1}{2}$	8	$-\frac{3}{2}$	785.49	2.21063	0.0443(-4)	-1350.4162	-58831.771
0	$-\frac{1}{2}$	15	$-\frac{1}{2}$	795.78	3.26791	0.077(-4)	1241.5109	-28774.333
3	$-\frac{1}{2}$	20	$-\frac{1}{2}$	809.84	3.06916	0.0068(-4)	1325.7147	-3441350.394
15	$+\frac{1}{2}$	35	$-\frac{3}{2}$	809.84	2.54902	1.3794(-4)	-11.0316	-69.939
15	$+\frac{1}{2}$	1	$-\frac{3}{2}$	836.8	2.96334	0.0021(-4)	-1307.332	-35049789.153
3	$-\frac{1}{2}$	35	$-\frac{3}{2}$	855.72	2.60257	0.0217(-4)	1393.3796	-287525.148
3	$-\frac{1}{2}$	9	$-\frac{1}{2}$	864.88	3.28173	3.1046(-4)	59.5006	-17.774
3	$-\frac{1}{2}$	28	$+\frac{1}{2}$	864.88	2.6326	0.0484(-4)	1380.6384	-58591.049
0	$-\frac{1}{2}$	22	$+\frac{3}{2}$	890.87	2.84638	0.0604(-4)	1307.8221	-40690.34
9	$-\frac{1}{2}$	4	$+\frac{3}{2}$	891.47	2.53488	0.0553(-4)	-1312.2205	-43333.721
3	$-\frac{1}{2}$	1	$-\frac{3}{2}$	918.17	3.01689	0.6066(-4)	97.0675	-427.967
16	$+\frac{3}{2}$	37	$+\frac{1}{2}$	926.21	2.17819	1.6199(-4)	-11.1239	-43.331
1	$+\frac{1}{2}$	29	$+\frac{3}{2}$	932.62	2.605	0.0031(-4)	1362.3745	-14293420.459
4	$+\frac{1}{2}$	11	$+\frac{3}{2}$	963.43	2.69264	2.707(-4)	59.5905	-19.182
5	$+\frac{3}{2}$	16	$+\frac{1}{2}$	992.78	2.09223	0.0215(-4)	1260.7352	-237378.209

$(\nu, L) = (0, 1)$		$(\nu', L') = (3, 1)$					$f_0 = 185483644.34501278$ MHz	
i	M_J	f	M'_J	B [μT]	$\Delta\alpha_{if}$	$\lvert\Theta^{if}_{\epsilon,n}\rvert$	Δf_{hf} [MHz]	Δf_{LS} [Hz]
9	$-\frac{1}{2}$	9	$-\frac{1}{2}$	0.44	2.66523	0.9844(-4)	-37.4044	-155.15
3	$-\frac{1}{2}$	3	$-\frac{1}{2}$	2.09	3.0881	1.2283(-4)	68.5122	-115.472
14	$-\frac{1}{2}$	14	$-\frac{1}{2}$	4.94	3.04111	0.9901(-4)	-35.7644	-175.005
15	$+\frac{1}{2}$	15	$+\frac{1}{2}$	5.0	3.04111	0.9787(-4)	-35.7644	-179.123
13	$-\frac{3}{2}$	13	$-\frac{3}{2}$	7.3	2.90015	0.263(-4)	-35.7645	-2365.737
16	$+\frac{3}{2}$	16	$+\frac{3}{2}$	7.61	2.90015	0.2286(-4)	-35.7645	-3129.587
16	$+\frac{3}{2}$	7	$+\frac{1}{2}$	7.71	2.90673	1.554(-4)	-108.8576	-67.901
10	$+\frac{1}{2}$	10	$+\frac{1}{2}$	8.46	2.66523	0.9749(-4)	-37.4044	-158.209
6	$-\frac{1}{2}$	13	$-\frac{3}{2}$	13.28	2.70564	1.5586(-4)	52.9456	-62.83
11	$+\frac{3}{2}$	11	$+\frac{3}{2}$	22.16	3.04111	1.0345(-4)	-37.4047	-160.319
14	$-\frac{1}{2}$	9	$-\frac{1}{2}$	39.35	2.451	0.6818(-4)	-29.5707	-297.41
9	$-\frac{1}{2}$	14	$-\frac{1}{2}$	39.81	3.25534	0.6802(-4)	-43.5976	-396.953
4	$+\frac{1}{2}$	4	$+\frac{1}{2}$	39.81	3.0881	1.2637(-4)	68.5122	-109.092
2	$-\frac{3}{2}$	10	$+\frac{1}{2}$	140.74	3.1755	0.0351(-4)	1374.7888	-145787.742
3	$-\frac{1}{2}$	1	$+\frac{1}{2}$	162.34	3.12095	1.7333(-4)	84.8456	-58.604
10	$+\frac{1}{2}$	2	$-\frac{3}{2}$	173.15	3.37658	0.0353(-4)	-1343.6615	-153031.952

Continued on next page

$(\nu, L) = (0, 1)$		$(\nu', L') = (3, 1)$					$f_0 = 185483644.34501278$ MHz	
i	M_J	f	M'_J	B [μT]	$\Delta\alpha_{if}$	$\lvert\Theta^{if}_{\epsilon,n}\rvert$	Δf_{hf} [MHz]	Δf_{LS} [Hz]
13	$-\frac{3}{2}$	8	$-\frac{3}{2}$	176.47	3.12145	1.8273(-4)	-29.7441	-52.737
1	$+\frac{1}{2}$	3	$-\frac{1}{2}$	177.56	2.11553	1.7319(-4)	48.9032	-39.791
8	$-\frac{3}{2}$	13	$-\frac{3}{2}$	178.95	2.81982	1.8619(-4)	-43.4197	-45.886
3	$-\frac{1}{2}$	15	$+\frac{1}{2}$	187.1	2.53084	0.0212(-4)	1368.7823	-317150.382
1	$+\frac{1}{2}$	15	$+\frac{1}{2}$	191.81	3.14823	0.0568(-4)	1349.1825	-55080.608
15	$+\frac{1}{2}$	1	$+\frac{1}{2}$	212.46	2.74606	0.0506(-4)	-1319.7342	-60427.814
0	$-\frac{1}{2}$	0	$-\frac{1}{2}$	212.46	2.85317	0.1893(-4)	65.2173	-4489.415
5	$+\frac{3}{2}$	14	$-\frac{1}{2}$	258.58	1.99527	0.0043(-4)	1368.9523	-5974746.079
6	$-\frac{1}{2}$	8	$-\frac{3}{2}$	266.07	2.26306	0.024(-4)	58.8796	-221974.978
0	$-\frac{1}{2}$	9	$-\frac{1}{2}$	329.92	2.55811	0.0294(-4)	1354.8186	-166933.649
14	$-\frac{1}{2}$	5	$+\frac{3}{2}$	330.8	3.80504	0.0031(-4)	-1336.275	-21966206.48
8	$-\frac{3}{2}$	6	$-\frac{1}{2}$	335.18	3.0674	0.0363(-4)	-116.3427	-131632.759
15	$+\frac{1}{2}$	3	$-\frac{1}{2}$	345.21	2.32975	0.0216(-4)	-1336.1035	-282210.403
16	$+\frac{3}{2}$	10	$+\frac{1}{2}$	401.49	3.49684	0.0995(-4)	-30.4327	-19916.6
15	$+\frac{1}{2}$	9	$-\frac{1}{2}$	423.26	3.65751	1.0754(-4)	-30.7575	-178.413
10	$+\frac{1}{2}$	16	$+\frac{3}{2}$	430.13	2.49141	0.1477(-4)	-42.6762	-6444.146

Continued on next page

$(\nu, L) = (0, 1)$		$(\nu', L') = (3, 1)$					$f_0 = 185483644.34501278$ MHz	
i	M_J	f	M'_J	B [μT]	$\Delta\alpha_{if}$	$\lvert\Theta^{if}_{\epsilon,n}\rvert$	Δf_{hf} [MHz]	Δf_{LS} [Hz]
0	$-\frac{1}{2}$	15	$+\frac{1}{2}$	431.6	2.26306	0.0527(-4)	1349.7117	-46021.681
9	$-\frac{1}{2}$	15	$+\frac{1}{2}$	442.49	2.04883	1.0654(-4)	-42.3668	-101.835
3	$-\frac{1}{2}$	9	$-\frac{1}{2}$	458.88	2.42422	0.0302(-4)	1373.8037	-150243.417
6	$-\frac{1}{2}$	6	$-\frac{1}{2}$	483.21	2.85317	0.0448(-4)	-20.1311	-80183.969
15	$+\frac{1}{2}$	0	$-\frac{1}{2}$	484.62	3.0674	0.0451(-4)	-1320.3824	-85095.859
9	$-\frac{1}{2}$	0	$-\frac{1}{2}$	496.1	2.96028	0.0315(-4)	-1326.8431	-168655.77
9	$-\frac{1}{2}$	3	$-\frac{1}{2}$	505.82	3.3291	0.028(-4)	-1342.5505	-240164.106
0	$-\frac{1}{2}$	3	$-\frac{1}{2}$	540.01	3.22199	1.8243(-4)	49.5341	-54.615
3	$-\frac{1}{2}$	0	$-\frac{1}{2}$	563.07	2.71928	1.8593(-4)	84.1478	-44.374
7	$+\frac{1}{2}$	10	$+\frac{1}{2}$	638.54	2.55811	1.1058(-4)	57.8505	-118.015
14	$-\frac{1}{2}$	8	$-\frac{3}{2}$	682.3	2.47728	1.6818(-4)	-31.8384	-49.411
10	$+\frac{1}{2}$	7	$+\frac{1}{2}$	702.72	2.96028	1.049(-4)	-115.2349	-151.757
8	$-\frac{3}{2}$	14	$-\frac{1}{2}$	717.43	2.47728	1.7112(-4)	-41.2965	-47.729
15	$+\frac{1}{2}$	3	$-\frac{1}{2}$	744.75	2.32975	0.028(-4)	-1336.0638	-167907.159
1	$+\frac{1}{2}$	9	$-\frac{1}{2}$	815.2	3.44328	0.0603(-4)	1353.9254	-53374.573
17	$+\frac{5}{2}$	17	$+\frac{5}{2}$	1000.0	2.61824	1.2306(-4)	-35.7642	-97.543

$(\nu, L) = (0, 0)$		$(\nu', L') = (3, 2)$					$f_0 = 190175354.34176856$ MHz	
i	M_J	f	M'_J	B [μT]	$\Delta\alpha_{if}$	$\lvert\Theta^{if}_{\epsilon,n}\rvert$	Δf_{hf} [MHz]	Δf_{LS} [Hz]
0	$-\frac{1}{2}$	4	$-\frac{5}{2}$	450	3.97192	2.831(-4)	34.7356	-26.593
1	$+\frac{1}{2}$	9	$+\frac{5}{2}$	450	3.97192	2.831(-4)	34.7234	-26.593

Table C.5: Nearly insensitive (E2) transitions in the 1 mT range between two para-H_2^+ levels. Here all the states considered are stretched states and thus pure. The sensitivity of the two transitions is constant in the entire range, it is $s_{if} = \pm 13.5615$ MHz/T. We have chosen to consider the states at $B = 450$ μT for the hyperfine shift. By knowing the sensitivity, this shift can be computed for any other field strength, but does not change much along the entire range.

Bibliography

[1] N. Schwegler, D. Holzapfel, M. Stadler, A. Mitjans, I. Sergachev, J.P. Home, and D. Kienzler *Trapping and Ground-State Cooling of a Single H_2^+*, Phys. Rev. Lett. **131**, 133003 (2023).

[2] M. Hesse and D. Baye, *Lagrange-mesh calculations of the ground-state rotational bands of the H_2^+ and D_2^+ molecular ions*, J. Phys. B: At. Mol. Opt. Phys. **36**, 139 (2003).

[3] M. M. Cassar and G. W. F. Drake, *High precision variational calculations for H_2^+*, J. Phys. B: At. Mol. Opt. Phys. **37**, 2485 (2004).

[4] V. I. Korobov, *Coulomb three-body bound-state problem: Variational calculations of nonrelativistic energies*, Phys. Rev. A **61**, 064503 (2000).

[5] V. I. Korobov, L. Hilico and J.-Ph. Karr, *Hyperfine structure in the hydrogen molecular ion*, Phys. Rev. A **74**, 040502(R) (2006).

[6] J.-Ph. Karr, F. Bielsa, A. Douillet, J. Pedregosa, V. I. Korobov, and L. Hilico, *Vibrational spectroscopy of H_2^+ : Hyperfine structure of two-photon transitions*, Phys. Rev. A **77**, 063410 (2007).

[7] J.-Ph. Karr, V. I. Korobov, and L. Hilico, *Vibrational spectroscopy of H_2^+ : Precise evaluation of the Zeeman effect*, Phys. Rev. A **77**, 062507 (2008).

[8] R.E. Moss, *Calculations for the vibration-rotation levels of H_2^+ in its ground and first excited electronic states*, Molecular Physics, **80(6)**, 1541–1554 (1993).

[9] V. I. Korobov, J. C. J. Koelemeij, L. Hilico, and J.-Ph. Karr, *Theoretical Hyperfine Structure of the Molecular Hydrogen Ion at the 1 ppm Level*, PRL **116**, 053003 (2016).

[10] J.-Ph. Karr, M. Haidar, L. Hilico, Z.-X. Zhong, and V. I. Korobov, *Higher-order corrections to spin-spin scalar interactions in HD^+ and H_2^+*, Phys. Rev. A **102**, 052827 (2020).

[11] M. Haidar, V. I. Korobov, L. Hilico, and J.-Ph. Karr, *Higher-order corrections to spin-orbit and spin-spin tensor interactions in hydrogen molecular ions: Theory and application to* H_2^+, Phys. Rev. A **106**, 022816 (2022).

[12] D. A. Steck, *Quantum and Atom Optics*, Department of Physics, University of Oregon, I Chapter 7

[13] J.-Ph. Karr et al, *Hydrogen molecular ions: new schemes for metrology and fundamental physics tests*, J. Phys.: Conf. Ser. **723**, 012048 (2016).

[14] J. Shen, A. Borodin and S. Schiller, *A simple method for characterization of the magnetic field in an ion trap using* Be^+ *ions*, Eur. Phys. J. D **68**, 359 (2014).

[15] M. Puchalski and K. Pachucki, *Fine and hyperfine splitting of the* $2P$ *state in Li and* Be^+, Phys. Rev. A **79**, 032510 (2009).

[16] N. Shiga, W. M. Itano, and J. J. Bollinger, *Diamagnetic correction to the* $^9Be^+$ *ground-state hyperfine constant*, Phys. Rev. A **84**, 012510 (2011).

[17] J.-Ph. Karr, H_2^+ *and* HD^+*: candidates for a molecular clock*, J. Mol. Spectrosc. **300**, 37 (2014).

[18] D. T. Aznabayev, A. K. Bekbaev and V. I. Korobov, *Magnetic dipole transitions in the* H_2^+ *ion*, Phys. Rev. A **108**, 052827 (2023).

[19] H. O. Pilón and D. Baye, *Quadrupole transitions in the bound rotational–vibrational spectrum of the hydrogen molecular ion*, J. Phys. B **45** 065101 (2012).

[20] D. James, *Quantum dynamics of cold trapped ions with application to quantum computation*, Appl. Phys. B **66**, 181–190 (1998).

[21] V. I. Korobov, P. Danev, D. Bakalov, and S. Schiller, *Laser-stimulated electric quadrupole transitions in the molecular hydrogen ion* $\boldsymbol{H}_2^+$, Phys. Rev. A **97**, 032505 (2018).

[22] D. Bakalov and S. Schiller, *The electric quadrupole moment of molecular hydrogen ions and their potential for a molecular ion clock*, Appl. Phys. B **114**, 213–230 (2014). With Erratum

[23] L. Hilico, N. Billy, B. Grémaud, D. Delande, *Polarisabilities, Light Shifts and Two-photon Transition Probabilities between* $J = 0$ *states of the* H_2^+ *and* D_2^+ *Molecular Ions*, J. Phys. B **34**, 491–507 (2001).

[24] S. Schiller, D. Bakalov, A. K. Bekbaev, and V. I. Korobov, *Static and dynamic polarizability and the Stark and blackbody-radiation frequency shifts of the molecular hydrogen ions H_2^+, HD^+, and D_2^+*, Phys. Rev. A **89**, 052521 (2014).

[25] D.T. Aznabayev, A.K Bekbaev, S.A. Zhaugasheva and V.I. Korobov, *Leading order relativistic corrections to the dipole polarizability of the hydrogen molecular ions*, J. Phys. B **50**, 025104 (2017).